

# Calibrating the Iowa Pore Index with Mercury Intrusion Porosimetry and Petrography

**Final Report**  
**October 2017**

**Sponsored by**

Iowa Department of Transportation (InTrans Project 15-553)

Midwest Transportation Center

U.S. Department of Transportation Office of the Assistant Secretary for Research and Technology



IOWA STATE UNIVERSITY  
Institute for Transportation

National Concrete Pavement  
Technology Center



## **About the National CP Tech Center**

The mission of the National Concrete Pavement Technology (CP Tech) Center is to unite key transportation stakeholders around the central goal of advancing concrete pavement technology through research, tech transfer, and technology implementation.

## **About MTC**

The Midwest Transportation Center (MTC) is a regional University Transportation Center (UTC) sponsored by the U.S. Department of Transportation Office of the Assistant Secretary for Research and Technology (USDOT/OST-R). The mission of the UTC program is to advance U.S. technology and expertise in the many disciplines comprising transportation through the mechanisms of education, research, and technology transfer at university-based centers of excellence. Iowa State University, through its Institute for Transportation (InTrans), is the MTC lead institution.

## **ISU Non-Discrimination Statement**

Iowa State University does not discriminate on the basis of race, color, age, ethnicity, religion, national origin, pregnancy, sexual orientation, gender identity, genetic information, sex, marital status, disability, or status as a U.S. veteran. Inquiries regarding non-discrimination policies may be directed to Office of Equal Opportunity, 3410 Beardshear Hall, 515 Morrill Road, Ames, Iowa 50011, Tel. 515-294-7612, Hotline: 515-294-1222, email [eooffice@iastate.edu](mailto:eooffice@iastate.edu).

## **Notice**

The contents of this report reflect the views of the authors, who are responsible for the facts and the accuracy of the information presented herein. The opinions, findings and conclusions expressed in this publication are those of the authors and not necessarily those of the Iowa Department of Transportation or the U.S. Department of Transportation (DOT).

This document is disseminated under the sponsorship of the U.S. DOT UTC program in the interest of information exchange. The U.S. Government assumes no liability for the use of the information contained in this document. This report does not constitute a standard, specification, or regulation.

The U.S. Government does not endorse products or manufacturers. If trademarks or manufacturers' names appear in this report, it is only because they are considered essential to the objective of the document.

## **Quality Assurance Statement**

The Federal Highway Administration (FHWA) provides high-quality information to serve Government, industry, and the public in a manner that promotes public understanding. Standards and policies are used to ensure and maximize the quality, objectivity, utility, and integrity of its information. The FHWA periodically reviews quality issues and adjusts its programs and processes to ensure continuous quality improvement.

## **Iowa DOT Statements**

Federal and state laws prohibit employment and/or public accommodation discrimination on the basis of age, color, creed, disability, gender identity, national origin, pregnancy, race, religion, sex, sexual orientation or veteran's status. If you believe you have been discriminated against, please contact the Iowa Civil Rights Commission at 800-457-4416 or the Iowa Department of Transportation affirmative action officer. If you need accommodations because of a disability to access the Iowa Department of Transportation's services, contact the agency's affirmative action officer at 800-262-0003.

The preparation of this report was financed in part through funds provided by the Iowa Department of Transportation through its "Second Revised Agreement for the Management of Research Conducted by Iowa State University for the Iowa Department of Transportation" and its amendments.

**Technical Report Documentation Page**

<b>1. Report No.</b> InTrans Project 15-553	<b>2. Government Accession No.</b>	<b>3. Recipient's Catalog No.</b>	
<b>4. Title and Subtitle</b> Calibrating the Iowa Pore Index with Mercury Intrusion Porosimetry and Petrography		<b>5. Report Date</b> October 2017	
		<b>6. Performing Organization Code</b>	
<b>7. Author(s)</b> Franciszek Hasiuk, Muhammad Firdaus Ahmed Ridzuan, and Peter Taylor		<b>8. Performing Organization Report No.</b> InTrans Project 15-553	
<b>9. Performing Organization Name and Address</b> Institute for Transportation Iowa State University 2711 South Loop Drive, Suite 4700 Ames, IA 50010-8664		<b>10. Work Unit No. (TRAIS)</b>	
		<b>11. Contract or Grant No.</b>	
<b>12. Sponsoring Organization Name and Address</b> Iowa Department of Transportation 800 Lincoln Way Ames, IA 50010 Midwest Transportation Center 2711 S. Loop Drive, Suite 4700 Ames, IA 50010-8664		<b>13. Type of Report and Period Covered</b> Final Report	
		<b>14. Sponsoring Agency Code</b> SPR RB08-016	
<b>15. Supplementary Notes</b> Visit <a href="http://www.cptechcenter.org">www.cptechcenter.org</a> and <a href="http://www.intrans.iastate.edu">www.intrans.iastate.edu</a> for color pdfs of this and other research reports.			
<b>16. Abstract</b> <p>The Iowa Pore Index (IPI) test is a fast, non-destructive, inexpensive, and environmentally friendly test used by several Midwestern state departments of transportation to determine the volume ratio of macropores to micropores in a coarse rock aggregate. When combined with x-ray diffraction and x-ray fluorescence, this method has been shown to be effective in predicting the performance of aggregates in portland cement concrete. The test has the potential to replace mercury porosimetry and be integrated into any petrophysical laboratory.</p> <p>This research aimed to understand the geological factors (depositional environment, facies, grain and pore types, texture, and paragenesis) responsible for the results of the IPI test. Samples of various geologic ages were collected around Iowa to represent different combinations of accepted and rejected porosity and clay contents. The pore index of each sample was calibrated quantitatively via helium and mercury porosimetry and qualitatively via thin section petrography.</p> <p>The findings show that even the most homogeneous sources have at least three different rock types. Petrographic analysis showed that limestones with a sparite matrix, peloidal grains, and a low matrix-to-allochem ratio (i.e., grainy) are better for road construction than limestones with a micrite matrix, skeletal grains, and a high matrix-to-allochem ratio (i.e., muddy). Dolostones with fine to coarse grains, crystal-supported euhedral to subhedral rhombs, and porous intercrystalline areas are more desirable than dolostones with very fine grains and a tightly interlocking crystal mosaic in anhedral form.</p> <p>Several linear models were developed to relate IPI to helium porosity. Limestones with a helium porosity less than ~7% and dolostones with a helium porosity greater than ~13% were found to be desirable for use in road construction. The critical range of pore-throat size was found to be between 0.02 and 0.1 μm. Coarse aggregates with modal pore throat sizes above this range were found to be desirable for use in road construction.</p>			
<b>17. Key Words</b> coarse aggregate—helium—mercury—porosity		<b>18. Distribution Statement</b> No restrictions.	
<b>19. Security Classification (of this report)</b> Unclassified.	<b>20. Security Classification (of this page)</b> Unclassified.	<b>21. No. of Pages</b> 66	<b>22. Price</b> NA



# **CALIBRATING THE IOWA PORE INDEX WITH MERCURY INTRUSION POROSIMETRY AND PETROGRAPHY**

**Final Report**  
October 2017

**Principal Investigator**  
Franciszek Hasiuk, Assistant Professor  
Geological and Atmospheric Sciences, Iowa State University

**Co-Principal Investigator**  
Peter Taylor, Director  
National Concrete Pavement Technology Center, Iowa State University

**Research Assistant**  
Muhammad Firdaus Ahmed Ridzuan

**Authors**  
Franciszek Hasiuk, Muhammad Firdaus Ahmed Ridzuan, and Peter Taylor

Sponsored by  
Iowa Department of Transportation,  
Federal Highway Administration,  
Midwest Transportation Center and  
U.S. Department of Transportation  
Office of the Assistant Secretary for Research and Technology

Preparation of this report was financed in part  
through funds provided by the Iowa Department of Transportation  
through its Research Management Agreement with the  
Institute for Transportation  
(InTrans Project 15-553)

A report from  
**National Concrete Pavement Technology Center**  
**Institute for Transportation**  
**Iowa State University**  
2711 South Loop Drive, Suite 4700  
Ames, IA 50010-8664  
Phone: 515-294-8103 / Fax: 515-294-0467  
[www.cptechcenter.org](http://www.cptechcenter.org) and [www.intrans.iastate.edu](http://www.intrans.iastate.edu)



## TABLE OF CONTENTS

ACKNOWLEDGMENTS .....	ix
EXECUTIVE SUMMARY .....	xi
INTRODUCTION .....	1
Deterioration Mechanism.....	1
Source Selection (Sampling Scheme).....	3
Rationale .....	6
METHODS .....	7
Iowa Pore Index Test .....	8
Helium Porosimetry .....	9
Mercury Porosimetry .....	11
X-ray Fluorescence .....	12
RESULTS .....	14
Rock Typing.....	14
Petrography .....	16
Helium Porosimetry .....	22
Mercury Injection Porosimetry .....	27
X-ray Fluorescence .....	30
DISCUSSION .....	32
Lithology Recategorization.....	32
Bulk Behavior .....	35
Rock Typing.....	36
Critical Pore-Throat Diameters.....	38
CONCLUSIONS.....	39
FURTHER STUDIES.....	40
REFERENCES .....	41
APPENDIX A: HELIUM POROSIMETRY DATA.....	45
APPENDIX B: XRF DATA.....	51

## LIST OF FIGURES

Figure 1. Ice segregation mechanism.....	3
Figure 2. Fifteen selected Iowa quarries .....	4
Figure 3. Workflow of aggregate pebbles performed at Iowa State University .....	7
Figure 4. Iowa Pore Index apparatus .....	9
Figure 5. Bulk density determination: (a) GeoPyc 1360 bulk volume analyzer (vertical orientation) and (b) DryFlo media with a sample uncompressed (left) then compressed (right) .....	10
Figure 6. (a) SEM image of Micromeritics DryFlo media and (b) DryFlo grain size distribution showing a modal diameter of 120 $\mu\text{m}$ .....	11
Figure 7. Source samples divided into different rock types.....	15
Figure 8. Limestone nomenclature: Folk (top) and Dunham (bottom) classifications .....	17
Figure 9. From left to right: Limestone sources under thin section, from low to high secondary IPI .....	18
Figure 10. (a) Porosity in skeletal fragments, occurring as separate vug/intraparticle porosity, moldic porosity, and microporosity; (b) Porosity in peloids, occurring primarily as micro-scale pores (microporosity) within the peloids .....	19
Figure 11. Dolomite fabric descriptor: (a) Nonplanar fabrics characterized by tightly packed anhedral crystals and irregular intercrystalline boundaries, (b) Planar-e fabrics characterized by euhedral crystals and clearly defined intercrystalline boundaries, (c) Planar-s fabrics characterized by subhedral to euhedral crystals with straight intercrystalline boundaries .....	20
Figure 12. Dolostone sources under thin section, from low secondary IPI (left) to high secondary IPI (right) .....	21
Figure 13. Different rock types occurring in different abundances and having different porosities .....	23
Figure 14. Positive linear correlation between helium porosity, weighted by rock type abundance, and total pore index, with an $R^2$ value of 0.80.....	24
Figure 15. Positive linear correlation between helium porosity, weighted by rock type abundance, and primary pore index, with an $R^2$ value of 0.76 .....	25
Figure 16. (a) Poor correlation between between helium porosity, weighted by rock type abundance, and secondary pore index when lithology is ignored as a factor; (b) Positive linear correlation between helium porosity, weighted by rock type abundance, and secondary pore index for limestones and negative linear correlation between helium porosity, weighted by rock type abundance, and secondary pore index for dolostones.....	26
Figure 17. Primary-to-secondary pore index ratio versus helium porosity .....	27
Figure 18. Large pore-throat diameters yielding low secondary Iowa IPI values .....	28



Figure 19. Clear trend distinguishing the high (red) and low (green) secondary IPI samples between 0.02 to 0.1 microns, with high secondary IPI samples (>30 mL) shown in red and low secondary IPI samples (<30 mL) shown in green.....30

Figure 20. Separation in alumina data between what the Iowa DOT considers to be high-alumina aggregates and low-alumina aggregates .....31

Figure 21. Helium porosity–IPI by lithology (homogeneous lithology, limestone-intermediate-dolostone, limestone-dolostone).....34

**LIST OF TABLES**

Table 1. Geological, chemical, and physical properties of coarse aggregate sources .....5

Table 2. Critical pore-sizes from literature sources .....29

Table 3. Helium porosity–IPI transform functions .....33

Table 4. Broad depositional environment–diagenesis rock types.....37



## **ACKNOWLEDGMENTS**

The research team would like to acknowledge the Iowa Department of Transportation for sponsoring this research using Federal Highway Administration state planning and research funds and the Midwest Transportation Center and U.S. Department of Transportation Office of the Assistant Secretary for Research and Technology for funding a small related project, which this final report also covers.



## EXECUTIVE SUMMARY

The Iowa Pore Index (IPI) test is a method employed by several Midwestern state departments of transportation to determine the volume ratio of macropores to micropores in a rock aggregate by means of water intrusion. This method, when combined with x-ray diffraction (to measure the dolomite mineral structure using the peak shift) and x-ray fluorescence (to measure the calcite-to-dolomite ratio and the clay content using alumina), has been shown to be effective in predicting the performance of aggregates in portland cement concrete.

In this test, 4.5 kilograms of oven-dried crushed carbonate is intruded with water progressively at 240 kilopascals (35 psi). Readings of intruded volume are taken at 1 and 15 minutes, corresponding to macropore and micropore volumes, respectively. The IPI test is interesting more broadly because it is fast, nondestructive, inexpensive, and environmentally friendly. Therefore, it has the potential to replace mercury porosimetry and be integrated into any petrophysical laboratory.

This research aimed to understand the geological factors (depositional environment, facies, grain and pore types, texture, and paragenesis) responsible for the results of the IPI test. End-member samples of various geologic ages were collected around Iowa to represent different combinations of favorable and unfavorable IPI and clay contents. The pore index of each sample was calibrated quantitatively via helium and mercury porosimetry and qualitatively via thin section petrography.

The findings of this research show that even the most homogeneous sources have at least three different rock types, or groups of pebbles characterized by distinctive physical and textural attributes observable in hand-specimens. Petrographic analysis showed that limestones with a sparite matrix, peloidal grains, and a low matrix-to-allochem ratio (i.e., grainy) are better for road construction than limestones with a micrite matrix, skeletal grains, and a high matrix-to-allochem ratio (i.e., muddy). Dolostones with fine to coarse grains, crystal-supported euhedral to subhedral rhombs, and porous intercrystalline areas are more desirable than dolostones with very fine grains and a tightly interlocking crystal mosaic in anhedral form.

Each rock type occurs in a different abundance and has a different porosity. Several linear models were developed to relate IPI to helium porosity. Limestones with a helium porosity less than ~7% and dolostones with a helium porosity greater than ~13% were found to be desirable for use in road construction. The critical range of pore-throat size was found to be between 0.02 and 0.1  $\mu\text{m}$ . Coarse aggregates with modal pore throat sizes above this range were found to be desirable for use in road construction.



## **INTRODUCTION**

Understanding the petrophysical nature of carbonate rocks has important implications for numerous stakeholders. To hydrogeologists, understanding carbonate pore systems is valuable for the detection of permeable and productive aquifers. To petroleum geologists, understanding carbonate pore systems means more efficient recovery of oil and gas reserves. To road builders and the taxpayers who fund them, understanding carbonate pore systems means smoother roads that last longer and cost less.

Indeed, fine and coarse aggregates (i.e., sand and crushed stone, respectively) constitute over 90% of asphalt cement concrete and 75% to 85% of portland cement concrete by weight, making these aggregates the largest line item when building roads. The Iowa Department of Transportation (DOT) spends approximately \$4 million per mile to repave a four-lane Interstate in rural areas, while the cost of reconstructing a two-lane highway in rural areas is \$1.3 million per mile (Iowa DOT 2004). In urban areas, the costs are even higher. To maximize the service lives of pavements under its jurisdiction, the Iowa DOT has used science-based methods for aggregate selection since the early 1900s and has committed itself to finding the most effective way of identifying aggregates that would lead to a prolonged lifespan of pavement roads.

This study evaluated one of the three tests used by the Iowa DOT to grade coarse aggregates. Developed in 1980 by James Myers and Wendell Dubberke (Myers and Dubberke 1980), the Iowa Pore Index (IPI) test has been used by several Midwestern state departments of transportation (e.g., Iowa, Michigan, and Kentucky) to rapidly and nondestructively determine the macropore-to-micropore ratio of coarse aggregate. The IPI test was recently accepted as an American Association of State Highway Transportation Officials (AASHTO) standard (AASHTO TP 120-16). This technique, when combined with x-ray diffraction (XRD) to measure the dolomite mineral structure (using the peak shift) and x-ray fluorescence (XRF) to measure the calcite-to-dolomite ratio and the clay content (using alumina), has been shown to be effective in predicting the performance of aggregates in portland cement concrete (Iowa DOT 2015).

The purpose of this study was to enhance the predictive power of IPI by understanding its geological basis. IPI data for different aggregate samples were compared with petrographic thin sections, helium porosity measurements, and mercury intrusion measurements taken from coarse aggregate pebbles within the same samples. The application of this method can be extended to other states and countries with similar bedrock and climate, including the Midwestern and Northeastern United States, Europe, and Central Asia, and the method can perhaps be applied in other industries that need a rapid, non-destructive analysis of the pore systems of large volumes of carbonate rock (e.g., the petroleum industry).

## **Deterioration Mechanism**

Pavement deterioration can be attributed to many causes, including expansive alkali-aggregate reaction (e.g., Okada et al. 1989, Owsiak et al. 2015, Mohr and Bryant 2016), thermal cycling (e.g., Schauer 1961, Al-Tayyib et al. 1989), acid attack (e.g., Woodson 2009, Yuan et al. 2013), traffic abrasion (e.g., Ghafoori 2007), faulty mix designs (e.g., imbalanced water-cement ratio),

and mechanical weathering from the freezing of water (i.e., frost weathering) (e.g., Sweet 1948, Litvan 1973, Salcedo 1984, Taber 1929).

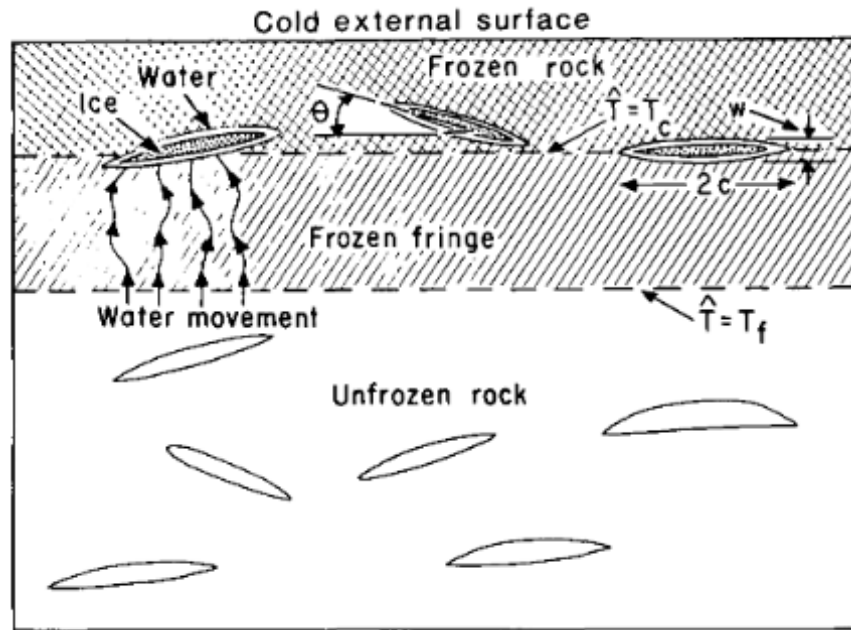
In many parts of Midwestern United States, the abundance of meteoric water coupled with the cold winter climate proves to be detrimental to the durability of concrete pavements (Myers and Dubberke 1980, Legg Jr. 1994, Riding et al. 2013). Successive freeze-thaw cycling is commonly thought to be the dominant mechanism responsible for the premature deterioration of highway pavements (e.g., D-cracking). However, the concrete pavement community's understanding of the fracturing mechanism has since evolved. Numerous studies (e.g., Taber 1929, Dash et al. 2006, Hallet 2006, Murton et al. 2006, Rempel 2007) involving limestones and other types of rock have shown that the volumetric expansion of water upon freezing is not as significant a contributor to cracking as is the continuous addition of fluid to the rock in subfreezing temperatures.

For the volumetric expansion of water to be responsible for frost weathering, over 91% of a pore would have to contain water (91% saturated) for there to be enough expansion during freezing to propagate a crack. This is because water expands by only about 9% when it freezes. The rock would also have to be frozen from all sides to prevent the outflow of water into adjacent pores or out of the rock through an unfrozen side. Such a combination of conditions, however, is difficult to find in nature (Hallet 2006) or in manmade pavements.

Experiments have also shown that fracturing has occurred at saturations below 65%, significantly lower than the threshold value of 91% (Murton et al. 2006). In addition, it would be expected that fracture growths occur in bursts each time temperatures fall below the freezing point of water (0°C) and that no fracture growth would occur at steadily subfreezing temperatures. However, research has shown that rapid fracturing occurs at a sustained, critical temperature range of -3°C to -6°C (Hallet 2006). Fluids that contract upon freezing should also not cause cracks to grow, yet such fluids (e.g., argon and helium) have been found to cause fracturing of porous materials (Taber 1929, Dash et al. 2006).

The most likely process responsible for frost weathering is ice segregation (Taber 1929, Dash et al. 2006, Hallet 2006, Murton et al. 2006, Rempel 2007), which involves the repulsive forces acting between the ice lens and the porous medium. These forces create a disjoining pressure between the two interfaces, leaving an interfering thin layer of water (a "pre-melted" film) that remains unfrozen (Dash et al. 2006). Because the temperature of the medium is colder near the surface than in the subsurface, a pressure gradient develops, resulting in capillary forces that draw water upwards (see Figure 1).





Walder and Hallet 1985, Reproduced with permission of the Geological Society of America via Copyright Clearance Center

**Figure 1. Ice segregation mechanism**

Water is continuously brought into the pore, causing the ice lens—and hence, the fracture—to grow steadily under sustained subfreezing temperatures. An appreciation of this mechanism can help improve understanding of the deterioration of concrete and other fabricated porous media due to ice and salt growth (Hallet 2006).

### Source Selection (Sampling Scheme)

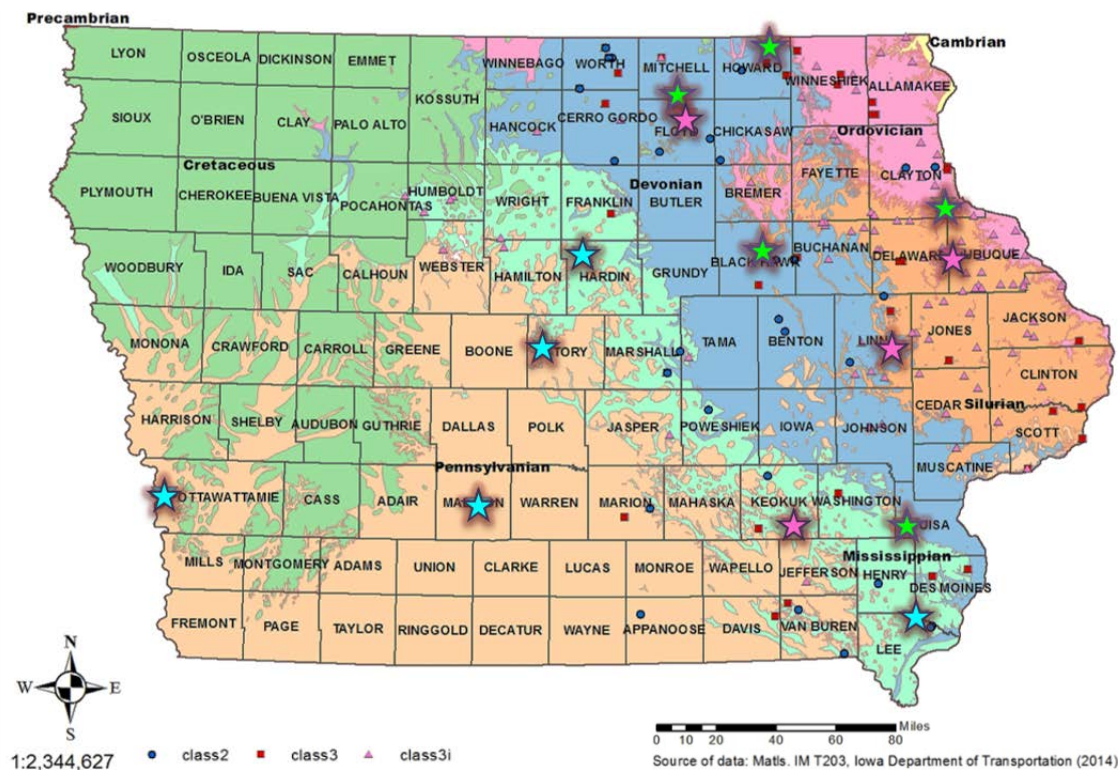
Historically, the Iowa DOT has graded aggregates for highway pavements based on their service history. Class 2 aggregates show minimal deterioration (less than 5%) on non-Interstate roads over 20 years, Class 3 aggregates show minimal deterioration on non-Interstate roads over 25 years, and Class 3i aggregates show minimal deterioration on Interstate highways over 30 years (Iowa DOT 2016). However, since the 1980s, advances in concrete technology and reconstruction techniques have made direct reliance on service history problematic. With myriad variables affecting concrete performance, it is difficult to judge the extent to which each variable affects concrete performance.

Therefore, the Iowa DOT has undertaken efforts to predict the service performance of aggregates based on their physical, chemical, and geological properties. Three main factors have been shown to affect the durability of Iowa coarse aggregates in portland cement concrete: mineral stability, clay content, and pore structure (Dubberke and Marks 1989, Iowa DOT 2015).

The first criterion, mineral stability, indicates the purity of the carbonate rock as determined by the XRD dolomite peak shift at a threshold value of 2.90 Å. The lower the peak shift, the greater

the stability of the dolomite mineralogy. Pure limestones and dolostones, as opposed to mixtures of the two, are generally found to produce longer-lasting pavements. Mixtures of calcite and dolomite (“intermediates”) are detrimental because they break down in the presence of deicing salts. The second criterion is the clay content of the aggregate, as determined by the aluminum oxide (Al<sub>2</sub>O<sub>3</sub>) fraction in XRF data. Clays such as illite and montmorillonite are undesirable for durability due to their expansive nature when exposed to water and their ability to hold water, which can feed ice segregation. Clays also provide ample surface area for chemical reactions. The third criterion is IPI, which measures the macropore-to-micropore ratio using water intrusion under constant pressure. Water does not drain as easily from small pores due to capillary forces, making aggregates with abundant small pores more susceptible to ice segregation processes.

For this study, coarse aggregates from 15 Iowa quarries, most of which were Ordovician to Mississippian in age, were selected to represent a spectrum of quality ratings based on the three aforementioned properties (Figure 2 and Table 1).



Class 2 aggregate sources are shown in blue dots; Class 3 aggregate sources are shown in red squares; Class 3i aggregate sources are shown in pink triangles; sources used in this study (shown as stars) were sampled from different geological formations, ages, and locations throughout Iowa

**Figure 2. Fifteen selected Iowa quarries**

**Table 1. Geological, chemical, and physical properties of coarse aggregate sources**

<b>Lithology</b>	<b>Porosity (secondary IPI)</b>	<b>Chemistry (alumina content)</b>	<b>Litho- Poro-Chem</b>	<b>Geologic Age</b>	<b>Formation</b>
Limestone	Low	Low	LGG1	Upper Devonian	Lime Creek Formation
Limestone	Low	Low	LGG2	Mississippian	Gilmore City Formation
Limestone	Medium	High	LMB	Mississippian	St. Genevieve Formation
Limestone	High	Low	LBG	Pennsylvanian	Swope: Bethany Falls Limestone
Limestone	High	High	LBB2	Pennsylvanian	Swope: Bethany Falls Limestone
Limestone	High	High	LBB1	Pennsylvanian	Hertha Limestone
Intermediate	Low	Low	IGG	Late Ordovician	Stewartville Foramtion
Intermediate	Low	Low	IGG (dol.)	Mid Devonian	Lithograph City Fm.: Osage Springs Mb.
Intermediate	Low	High	IGB1	Devonian	Cedar Valley Group
Intermediate	Low	High	IGB2	Mississippian	Maynes Creek Fm.: Wassonville Mb.
Intermediate	High	High	IBB	Mid Devonian	Little Cedar Fm.: Solon Mb.
Dolostone	Low	Low	DGG1-	Silurian	Hopkinton Formation
Dolostone	Low	Low	DGG2	Silurian	Gower: Anamosa
Dolostone	High	Low	DBG	Mississippian	Maynes Creek Fm.: Wassonville Mb.
Dolostone	High	High	DBB	Mid Devonian	Cedar Valley Group: Coralville Mb

For example, IGB2 is an intermediate source with low microporosity and high alumina content. Because samples came from active quarries, sample choices were weighted toward favorable aggregate properties (i.e., low micropores and alumina). Therefore, it was not possible to find certain combinations of properties, i.e., an intermediate source with high microporosity and low alumina content or a dolostone with low microporosity and high alumina content.

## **Rationale**

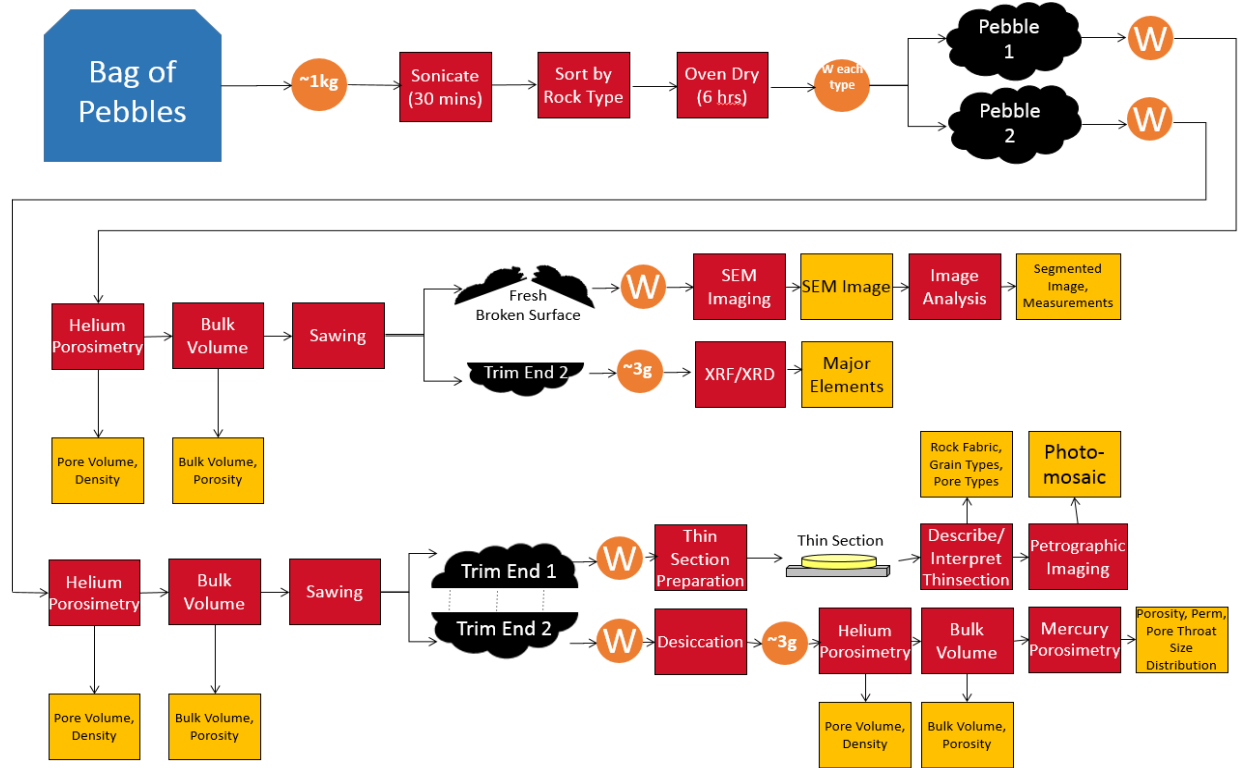
IPI has several advantages over traditional petrophysical methods that measure the porosity and pore-size distribution of reservoir rocks (e.g., mercury intrusion porosimetry):

1. Only water and air are required to analyze a sample. The IPI does not use any chemicals or other hazardous materials (e.g., mercury, alcohol) and hence poses little environmental hazard. These simple consumables make the test relatively inexpensive.
2. It is nondestructive. Samples tested using the IPI largely maintain their integrity in shape, volume, and weight after each testing. Thus, they can be retested at a later date or subsampled for further testing (e.g., petrographic thin sections).
3. It is relatively quick; each test takes only 30 minutes. Another commonly used method, ASTM C666, which evaluates the resistance of concrete to rapid freezing and thawing in water (Procedure A) or freezing in air and thawing in water (Procedure B), can take up to five months to complete the mandated 300 testing cycles.
4. It investigates a significant amount of rock (4.5 kg), which improves the comparability of the results to the quarry or reservoir scale as opposed to methods using smaller samples like core plugs.
5. It uses crushed rock instead of a whole core. Crushing the rock allows the intruding liquid to fully and quickly permeate the rock's pore system. In addition, this may make IPI an applicable method for analyzing well-cuttings, a common byproduct of drilling.

For these reasons, the Iowa Pore Index is considered a viable and attractive alternative to other porosimetric methods.

## METHODS

Coarse aggregate samples were run through a uniform workflow for quantitative and qualitative analyses (Figure 3). These included IPI, XRF, XRD, thin section petrography, helium porosimetry, and mercury porosimetry. Scanning electron microscope (SEM) samples were prepared but not tested at this point because the required equipment was not yet available.



**Figure 3. Workflow of aggregate pebbles performed at Iowa State University**

The samples were collected from quarry stockpiles by Iowa DOT district officials. Iowa DOT geologists also provided stratigraphic sections describing each source's stratigraphy. IPI, XRD, and XRF analyses were performed at the Iowa DOT Materials Research Laboratory. All other analyses were performed at the Iowa State University Petrographic Industrial Research Laboratory (PIRL) in the Department of Geological and Atmospheric Sciences.

At PIRL, approximately 1 kg was extracted from each 4.5 kg sample and sonicated for 30 minutes to remove particles adhering to the surfaces of the aggregate pebbles. The wet pebbles were sorted into different rock types (RTs), or different groups of pebbles characterized by physical and textural appearance (i.e., color, surface texture, and recurrent associations of non-carbonate particles). After separation, the rock types were oven-dried at 135°C for 6 hours, and the oven-dried weight of each rock type was recorded.

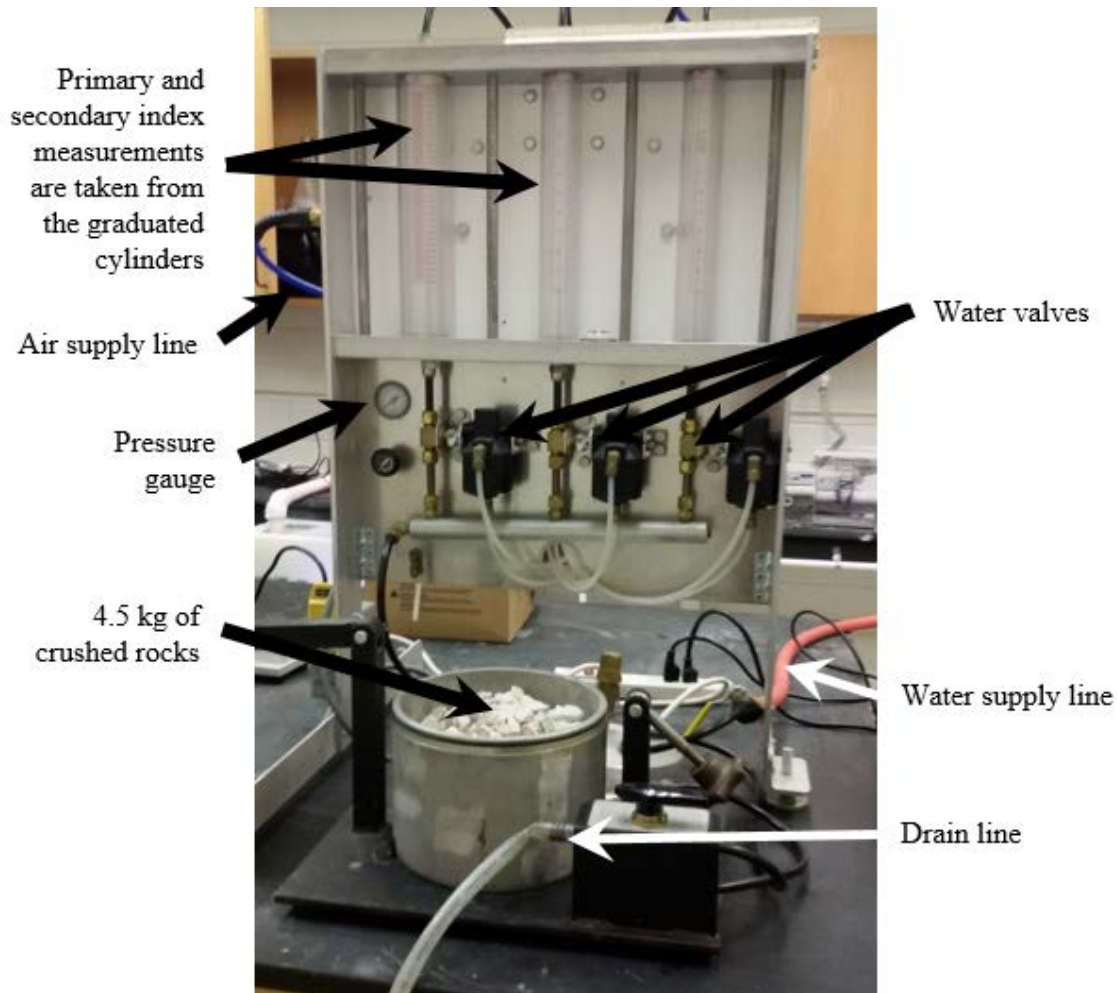
The rock types were labelled according to abundance. For example, in a given sample, RT01 was the rock type with the greatest abundance, RT02 had the second greatest abundance, and so on.

The characteristics of each rock type were different within each source and may have differed from one source to another. For example, RT01 from Source A may not have had the same geological characteristics or properties as RT01 from Source B.

Two pebbles were selected from each rock type and subsequently analyzed quantitatively via XRF, helium porosimetry, and mercury intrusion porosimetry and qualitatively via thin section petrography. The reason for selecting two pebbles was that a single pebble did not provide enough material to perform all analyses. Because the color, the reactivity to diluted 10% hydrochloric acid, and the helium porosity results of both pebbles closely approximated each other, we were confident that the two pebbles from each rock type were similar enough to be good representatives of the rock types.

### **Iowa Pore Index Test**

IPI records how much water intrudes into the pore network of a coarse aggregate sample under pressure after 1 and 15 minutes (Myers and Dubberke 1980, AASHTO TP 120-16). It is thought to relate roughly to the macropore-to-micropore ratio of the aggregate. To prepare for this test, 4.5 kg of crushed aggregate with a nominal maximum aggregate size of 12.5 to 19 mm (0.5 to 0.75 in.) was oven-dried for 6 hours at 135°C and desiccated at room temperature for 24 hours. A recent study (Gustafson et al. 2015) has also allowed the use of smaller particle sizes (9.5 to 12.5 mm or 3/8 to 0.5 in., and 4.8 to 9.5 mm or No. 4 to 3/8 in.) when a correction factor is applied. Then, the aggregate sample was placed in a closed container and intruded with tap water at a constant pressure of 35 psi, or ~240 kPa (Figure 4).



**Figure 4. Iowa Pore Index apparatus**

After the first and fifteenth minutes, the volume of water intruded was measured. These measurements are termed the primary and secondary indices, according to the method. These indices correspond to the volumes of water intrusion assumed to occupy the macropores and micropores of the aggregate sample, respectively.

### **Helium Porosimetry**

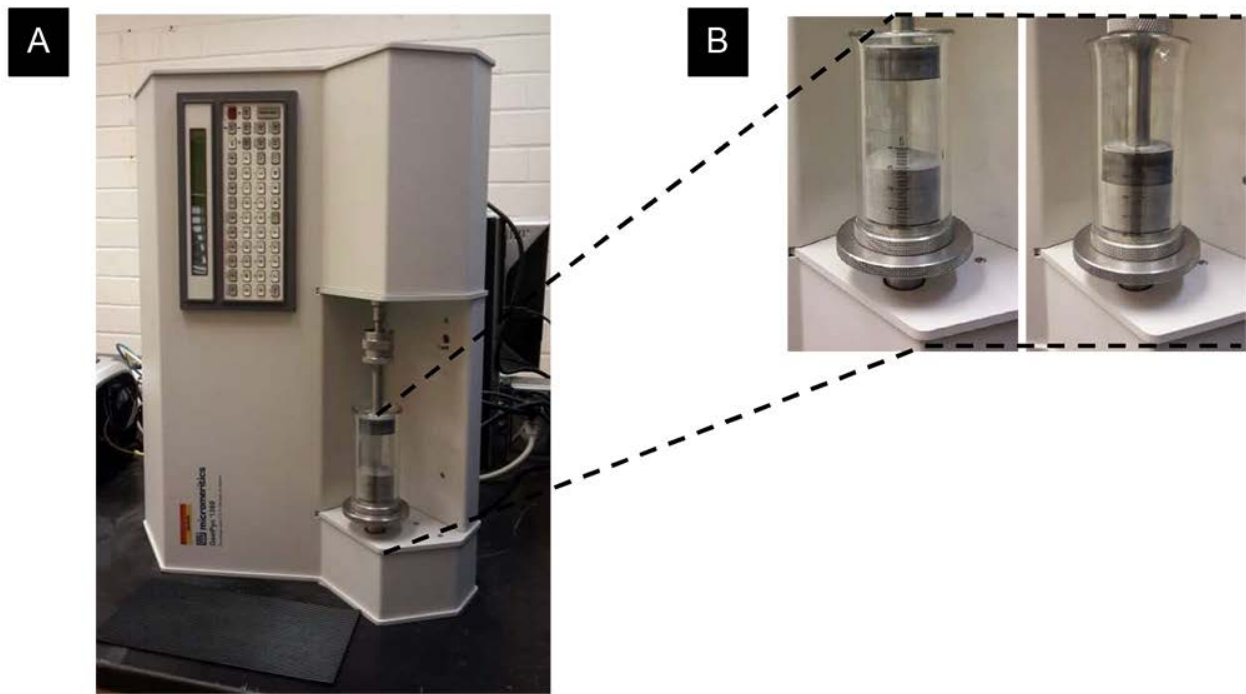
Helium porosimetry is based on combining a measurement of grain volume with bulk volume to calculate porosity (fraction of a solid that is void). The process consists of three steps: weighing the sample, obtaining its grain density via helium pycnometry, and obtaining its bulk volume. In this study, the weight of each pebble was measured using a Mettler Toledo ME204E analytical balance to a precision of 0.0001 g.

The calculation of grain density is based on Boyle's Law ( $P_1V_1 = P_2V_2$ ), where a known volume of helium gas at a fixed pressure is isothermally expanded into an unknown void volume. After expansion, the resultant stabilized pressure is measured and the grain volume (sometimes



referred to as skeletal volume) is calculated. Grain density (i.e., the density of the solid material excluding any open pores) was measured for each aggregate pebble using a Micromeritics AccuPyc II 1340. Each pebble was purged (filled and vented) with helium gas for 10 cycles before grain density measurements were recorded as the average of 5 to 10 cycles. To maintain a high degree of precision, the maximum standard deviation allowed for the grain volume measurement was  $0.0035 \text{ cm}^3$ . If a higher standard deviation was recorded, the test was repeated for the same sample until the standard deviation was below the aforementioned limit.

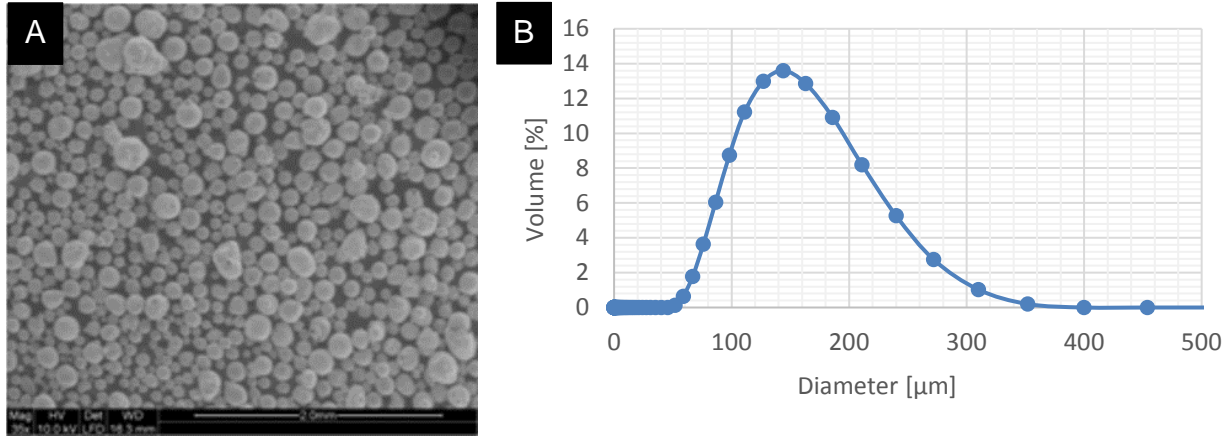
Measuring the envelope density (also referred to as the bulk density) of a pebble is not straightforward due to the pebble's irregular shape. To overcome this obstacle, samples were analyzed in an envelope density analyzer (Micromeritics GeoPyc 1360), which compresses irregularly shaped objects in a granular medium to measure envelope density (Figure 5).



**Figure 5. Bulk density determination: (a) GeoPyc 1360 bulk volume analyzer (vertical orientation) and (b) DryFlo media with a sample uncompressed (left) then compressed (right)**

The granular media (Micromeritics DryFlo) consisted of a mixture of graphite, aluminum oxide, and crystalline silica (quartz) with a modal diameter of  $120 \mu\text{m}$  (Figure 6).





Left: Edwards et al. 2011, © TMS (The Minerals, Metals & Materials Society) 2011, with permission of Springer

**Figure 6. (a) SEM image of Micromeritics DryFlo media and (b) DryFlo grain size distribution showing a modal diameter of 120 μm**

Displacement data were measured and recorded for 15 compression-decompression cycles. The parameters specified for this method were as follows: a chamber diameter of 38.1000 mm, a consolidation force of 90.0000 N, and a conversion factor of 1.2285 cm<sup>3</sup> pebble volume per mm linear displacement of the plunger. To maintain a high degree of precision, the maximum standard deviation allowed for the volume was 0.0120 cm<sup>3</sup>. If a higher standard deviation was recorded, the test was repeated for the same sample until the standard deviation was below the aforementioned limit. The GeoPyc 1360 was used in a vertical orientation to ensure that the long axis of the pebble did not align with the piston axis of the device and prevent full compression (Figure 5a).

Using the grain density from the helium pycnometer, the GeoPyc 1360 calculated the porosity of each sample using the following equation:

$$\varphi = \frac{\rho_e - \rho_s}{\rho_s} \times 100 \quad (1)$$

where  $\varphi$  is the helium porosity in percent by volume,  $\rho_e$  is the envelope density from the GeoPyc 1360, and  $\rho_s$  is the grain density from the AccuPyc II 1340.

### Mercury Porosimetry

Mercury porosimetry involves injecting mercury into an evacuated sample at increasing pressures to measure the volume fraction of increasingly smaller pore throats (Washburn 1921). The volume of mercury injected at each pressure step determines the non-wetting mercury saturation and, hence, the porosity in the sample at the pore-throat size that corresponds to that pressure step. This method is advantageous because it is quick (it takes about an hour to analyze a sample), can evaluate pore-throat sizes across a large size range from ~1 mm to ~3 nm, can take measurements from irregularly shaped samples, and gives reasonably accurate information on capillary entry pressure and pore geometry.

This method is governed by the Washburn equation for non-wetting liquid penetration (LP) (Washburn 1921):

$$D = \frac{4\gamma\cos\theta}{P} \quad (2)$$

where  $D$  is the pore-throat diameter (in  $\mu\text{m}$ ),  $P$  is the applied pressure (in pascals),  $\gamma$  is the surface tension of the mercury, and  $\theta$  is the contact angle between the mercury and the sample.

In this study, a Quantachrome PoreMaster 33 was used to measure the pore-throat size distributions. Each sample was oven-dried for 6 hours at  $135^\circ\text{C}$  and stored in a desiccator at room temperature for 24 hours before being analyzed. Mercury intrusion was conducted at  $24^\circ\text{C}$  to  $28^\circ\text{C}$ . A penetrometer with a stem volume of  $0.5\text{ cm}^3$  was used for pebbles with pore volumes less than  $0.35\text{ cm}^3$  (as determined by helium porosimetry), while a penetrometer with a stem volume of  $2\text{ cm}^3$  was used for pebbles with pore volumes greater than  $0.35\text{ cm}^3$ . The following parameters were specified: a mercury contact angle of  $140.00^\circ$  (intrusion and extrusion), a mercury surface tension of  $480.00\text{ erg/cm}^2$ , fine evacuation until 2 minutes (LP experiment), coarse evacuation until 3 minutes (LP experiment), and fill contact pressure of +1 to +3 psi ( $\sim$ +7 to +21 kPa, LP experiment).

Because of the large size of the sample cell, the mercury must be pressurized to completely fill the cell before analysis can begin. The higher the fill contact pressure, the smaller the maximum pore-throat size that can be recorded (i.e., data on the largest pore-throats are lost). However, if the fill contact pressure is too small, the mercury will not completely fill the sample chamber, and the machine will erroneously report air in the chamber as large pores in the rock. The standard procedure calls for a 2 psi ( $\sim$ 14 kPa) fill contact pressure to measure pore-throat diameters of  $100\text{ }\mu\text{m}$  and smaller. However, it was found that this pressure was too small to fill in the sample chamber, and therefore the fill contact pressure was increased to 3 psi ( $\sim$ 21 kPa). This translates to a largest pore-throat diameter of  $\sim$ 50  $\mu\text{m}$ . It should be noted that pores  $>5\text{ }\mu\text{m}$  can also be seen on thin sections, and hence there is an overlap between the two methods. The Quantachrome PoreMaster 33 attained a maximum pressure of 33,000 psi ( $\sim$ 230 MPa), which is equivalent to the smallest pore-throat diameter of 6 nm.

## **X-ray Fluorescence**

XRF is an analytical technique used to determine the bulk elemental composition of the aggregates. An X-ray beam is emitted to excite and displace electrons in the inner orbital shells of the atoms in a sample, releasing a burst of energy (or fluorescent X-rays) characteristic of different elements (Dubberke and Marks 1989). The electron displacement occurs when the energy of the beam exceeds the energy binding the electrons in their orbit.

For this test, the aggregates were oven-dried overnight at  $110^\circ\text{C}$  and powdered to less than a 200 mesh size (0.0029 in. or  $74\text{ }\mu\text{m}$ ). The samples were analyzed using an Axios X-ray Spectrometer at the Iowa DOT Materials Research Laboratory.

XRF is used mainly to identify the presence of alumina, which corresponds to the clay content of the aggregate. Elevated sulfur (resulting from pyrite) and manganese content has been shown to be particularly detrimental to the durability of dolostones, whereas elevated strontium content (>0.050%) is detrimental to the durability of limestones (Dubberke and Marks 1989).

## **RESULTS**

### **Rock Typing**

Results of sonicating the aggregates revealed that even the most homogeneous-looking source had at least three different rock types, or groups of pebbles characterized by distinctive physical and textural appearances observable at hand-specimen scales. For example, IGG, an intermediate source with a low secondary IPI (good porosity) and low alumina content (good chemistry), had five different rock types: RT1A was yellow and non-porous, RT1B was yellow and porous, RT02 was light grey, RT03 was dark grey, and RT04 was brown (Figure 7).

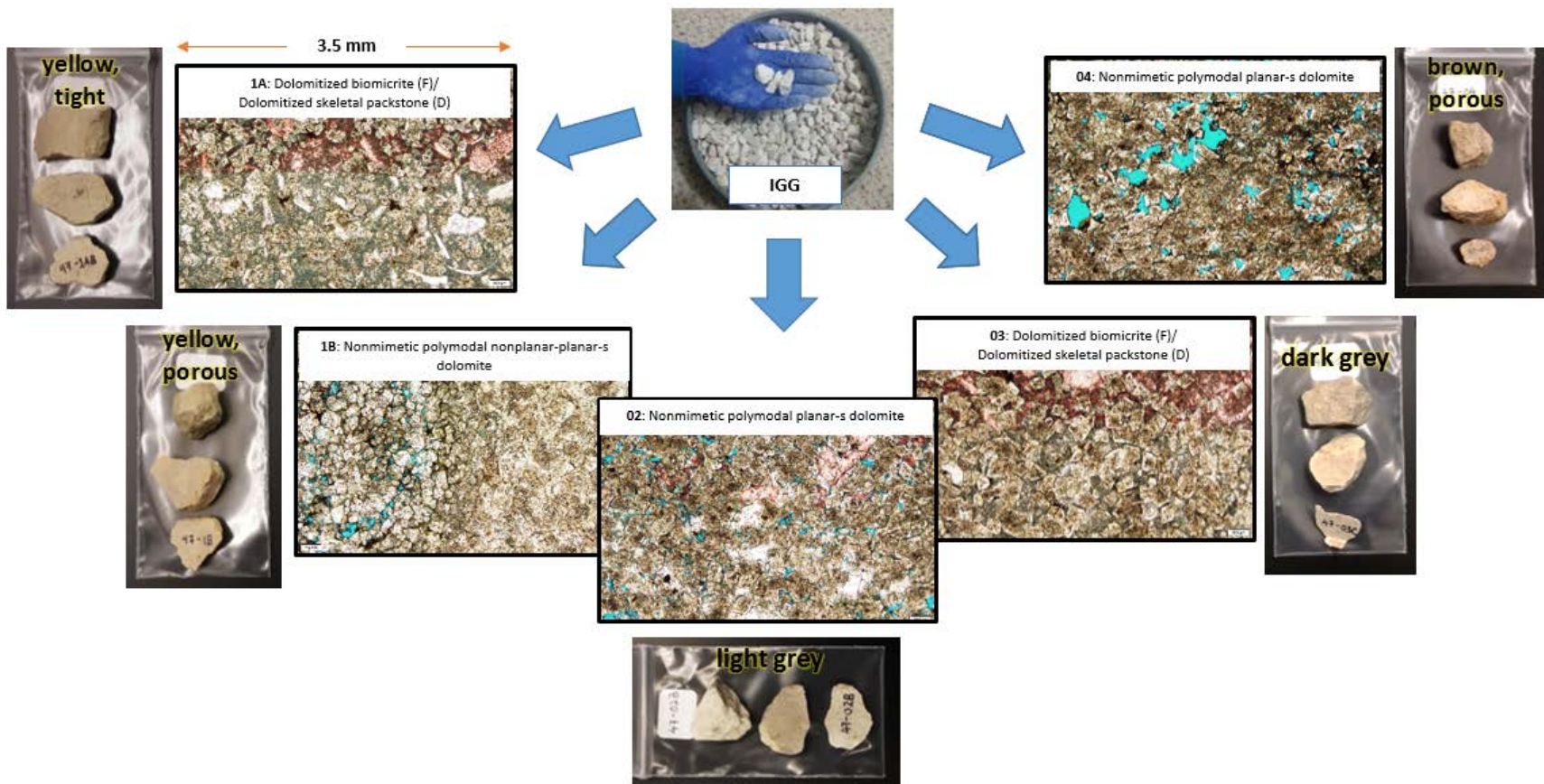


Figure 7. Source samples divided into different rock types

The rock types were labelled according to their abundance by weight, with RT01 being the most abundant rock type, followed by RT02, etc. Rock types that occurred in minimal quantities by weight (less than or equal to 3% oven-dried weight) were categorized as “Odd.” Due to their low abundance, no tests were performed on these rock types. However, these odd samples may affect the bulk properties of the aggregates and thus may contribute to either beneficial or deleterious concrete performance. However, any effect would likely be localized rather than pervasive due to their low abundance. Further study may be needed to assess the extent to which these odd rock types affect portland cement concrete performance.

For each source that contained odd rock types, the proportion by oven-dried weight of the remaining rock types was normalized to 100% (Appendix A). For example, Geode Quarry contained 51% RT01, 46% RT02, and 3% odd RT. After normalizing by removing the odd samples, the proportions of RT01 and RT02 became 53% and 47%, respectively. Failure to normalize the rock types would lead to incorrect results when calculating bulk sample properties.

## **Petrography**

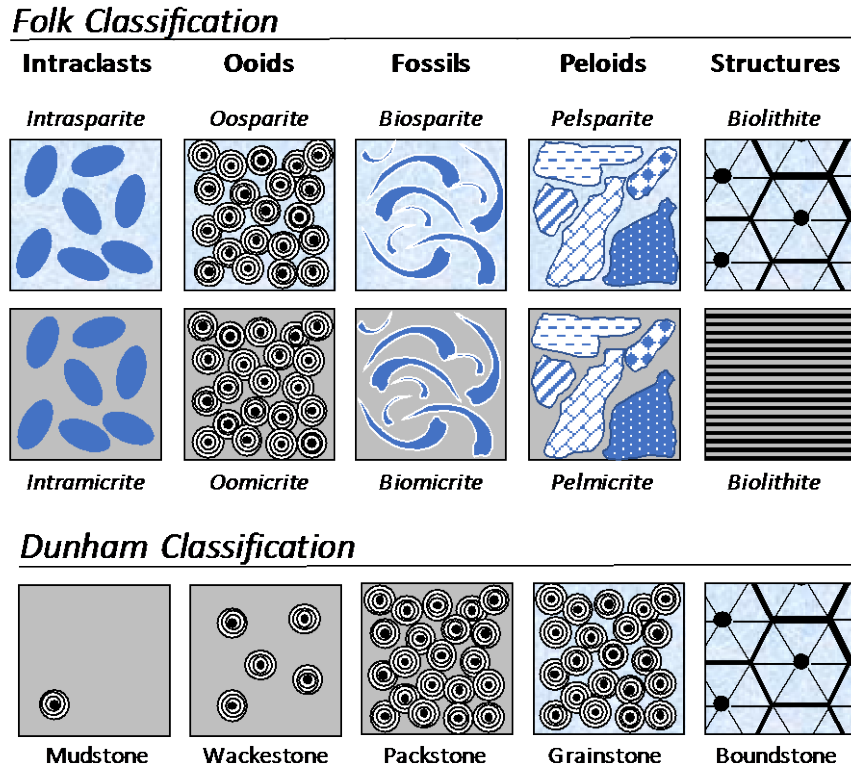
The other half of the pebble used for mercury porosimetry was used to make a petrographic thin section (30  $\mu\text{m}$  thick). The Iowa DOT classifies aggregate sources into three groups: limestones, dolostones, and intermediates (i.e., mixtures of limestone and dolostone). All thin sections were stained with alizarin red S to distinguish the mineral calcite from dolomite. When exposed to the dye, the calcite grains stained red while the dolomite and other grains remained unaffected. Thin sections were also stained with potassium ferricyanide to identify iron-rich calcite. The thin section descriptions were based on the modal grain size and textural properties of the sample.

Based on the petrographic analyses, it was found that the proportion of calcite to dolomite was highly variable within the intermediate sources. Therefore, to allow generalization, we simplified the lithology further and classified the sources into only two groups: limestones and dolostones. The intermediates, which consisted of both limestones and dolostones, were assigned to one of the two groups based on the dominant lithology in each source, as seen in the thin sections. For example, IGG (dolostone) that contained 72% dolostone (RT01, RT03, RT04) and 28% limestone (RT02) was categorized as a (dominantly) dolostone source. Similarly, IGB1 and IGB2 were categorized as (dominantly) dolostone sources, while IGG and IBB were categorized as (dominantly) limestone sources.

Because rock types occurred in different abundances and had different porosities, the thin sections used to exemplify the sources were selected based on the highest weighted porosity of the rock types (cf. Helium Porosimetry below). For example, the weighted porosities for RT01 and RT02 from Crescent (Bethany Falls) were 6.8% and 0.7% respectively, and hence thin section RT01 was chosen for this source.

*Limestones*

Limestones were described using both Folk (1959, 1962) and Dunham (1962) classifications (Figure 8).



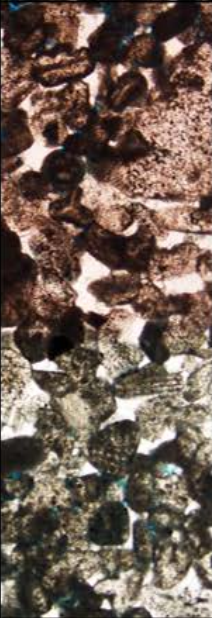
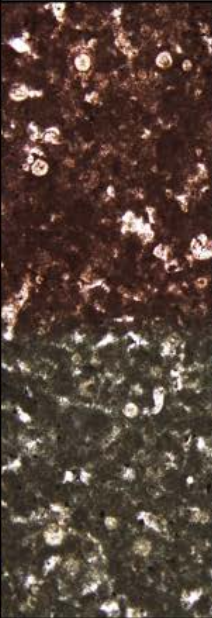
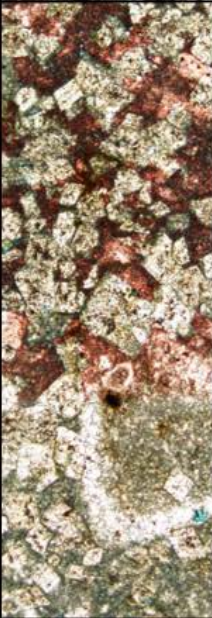
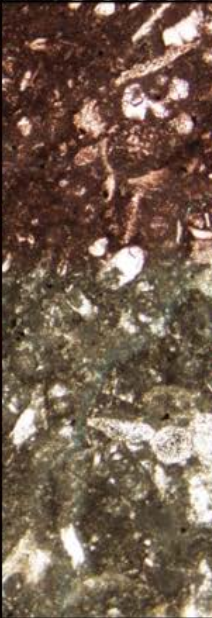
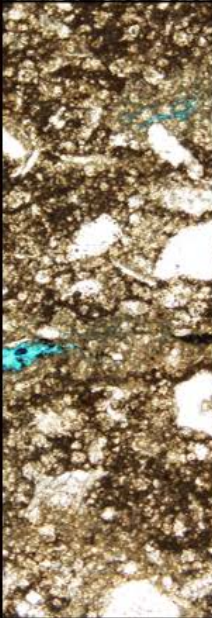



**Figure 8. Limestone nomenclature: Folk (top) and Dunham (bottom) classifications**

The Folk classification system describes limestone based on the type of grains present in the rock. The system pairs a prefix describing the allochem (grain type) and a suffix describing the orthochem (the matrix binding the allochems together). The allochems include ooids (spherical, layered calcite grains), peloids (spherical to ovoid carbonate grains that lack internal structure), bioclasts (biological or fossil fragments), and intraclasts (fragments of carbonate rocks from elsewhere). The orthochem can be divided into sparite (coarsely crystalline calcite) and micrite (microcrystalline calcite).

The Dunham classification system describes limestone based on its depositional texture, i.e., the grain-to-matrix ratio. Matrix-supported limestone with less than 10% grains is called mudstone; mud-supported limestone with greater than 10% grains is called wackestone. Grain-supported limestone with greater than 10% grains is called packstone; grain-supported limestone with no mud is grainstone. Limestones with original components bound together during deposition are classified as boundstone.

A correlation was found between the rock texture, as seen from the thin sections, and the secondary IPI for limestones (Figure 9).



(a)	(b)	(c)	(d)	(e)	(f)	(g)	(h)
							
F:Biopelsparite D: Crinoidal peloidal grainstone	F:Biopelmicrite D: Peloidal packstone	F: Dolomitized biomicrite D: Dolomitized skeletal packstone	F: Biomicrite D: Skeletal packstone	F: Intramicrite D: Skeletal packstone	F: Biomicrite D: Skeletal packstone	F: Biomicrite D: Skeletal packstone	F: Biomicrite D: Skeletal packstone
LGG2 2° IPI: 11	LGG1 2° IPI: 13	IGG 2° IPI: 20	LMB 2° IPI: 32	IBB 2° IPI: 38	LBG 2° IPI: 44	LBB2 2° IPI: 58	LBB1 2° IPI: 88

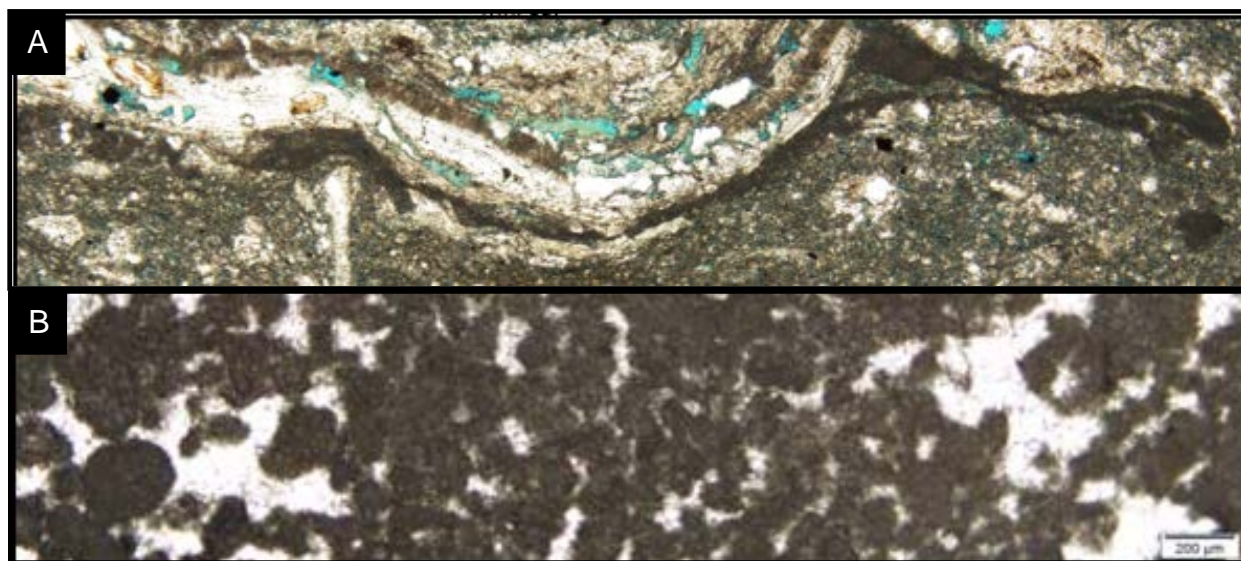
F = Folk, D = Dunham. Limestones with a sparite matrix, peloidal grains, and low matrix-to-allochem ratio (i.e., grainy) have lower secondary IPI than limestones with a micrite matrix, skeletal grains, and high matrix-to-allochem ratio (i.e., muddy)

**Figure 9. From left to right: Limestone sources under thin section, from low to high secondary IPI**



The following trends were observed. First, with regards to the matrix, sparite has a lower secondary IPI than micrite (see Figure 9a versus 9b through 9h). Micrite, or microcrystalline calcite, is formed as a result of the erosion of coarser carbonate grains or as precipitates in a low-energy environment (Folk 1959, 1962). Sparite (calcite cement), in contrast, is typically formed in a high-energy environment as a result of neomorphism through dissolution and recrystallization. The original precursor micrite particles are dissolved and replaced by a tightly interlocking crystalline mosaic with little intercrystalline porosity (Ahr 2011). This causes a sparite matrix to have less porosity than a micrite matrix.

Second, with regards to the allochem composition, peloidal limestones have a lower secondary IPI than skeletal limestones (see Figure 9a and 9b versus 9c through 9h). Peloid is a “term of ignorance” used to categorize allochems composed of accumulated carbonate mud or calcium carbonate precipitates (Scholle and Ulmer-Scholle 2003). Skeletal limestones are those composed of biological fossil fragments bound together by a matrix. The difference in porosity between the two allochems likely has to do with the type of porosity present. Peloids are composed primarily of micrite with intraparticle porosity; skeletal fragments are also associated with interparticle porosity (Figure 10).

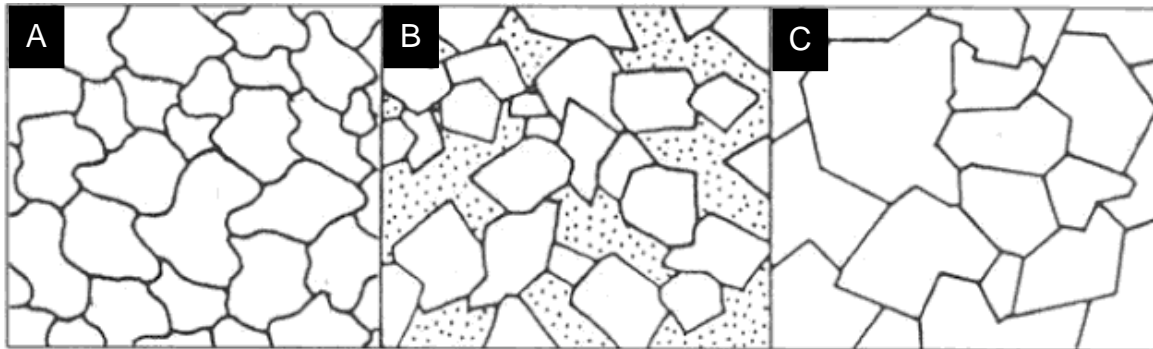


**Figure 10. (a) Porosity in skeletal fragments, occurring as separate vug/intraparticle porosity, moldic porosity, and microporosity; (b) Porosity in peloids, occurring primarily as micro-scale pores (microporosity) within the peloids**

Third, with regards to the allochem-to-matrix ratio, grainier samples (i.e., those with high allochem-to-matrix ratios) have a lower secondary IPI than muddier samples (cf. the progression of increasing muddiness from left to right in Figure 9b through 9h). This suggests that most pores contributing to the secondary IPI originated from the matrix and not as many originated from the grains. This is likely to be a function of the difference in the clay content of the lime mud matrix compared to that of the grains. XRF chemistry reveals that the greater the amount of matrix, the higher the alumina content of the aggregate (Appendix B).

## *Dolostones*

The textural trend in the dolostone thin sections is not as obvious. The dolostones were described according to Sibley and Gregg's (1987) classification. This system includes classification by textural fabrics (nonplanar, planar-e, or planar-s) (Figure 11), distribution of crystal size (unimodal or polymodal), and the degree of depositional fabric retention (mimetic or non-mimetic).



Scholle and Ulmer-Scholle 2003, © 2003 American Association of Petroleum Geologists;  
image adapted from Flügel 2004

**Figure 11. Dolomite fabric descriptor: (a) Nonplanar fabrics characterized by tightly packed anhedral crystals and irregular intercrystalline boundaries, (b) Planar-e fabrics characterized by euhedral crystals and clearly defined intercrystalline boundaries, (c) Planar-s fabrics characterized by subhedral to euhedral crystals with straight intercrystalline boundaries**

None of the dolostone samples examined in this study retained their primary fabric (i.e., they were all non-mimetic). Furthermore, sources with similar secondary IPI (i.e., Columbus Junction IGB2, DGG1, IGG [dolostone], and IGB1) displayed markedly different textures (Figure 12).




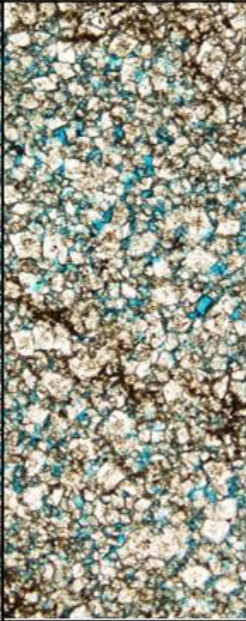
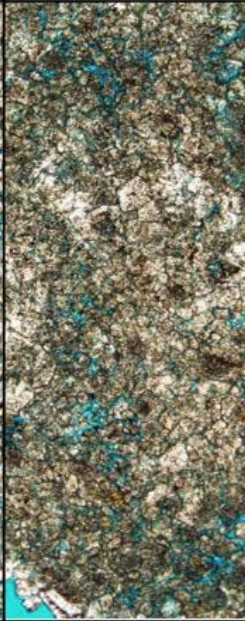

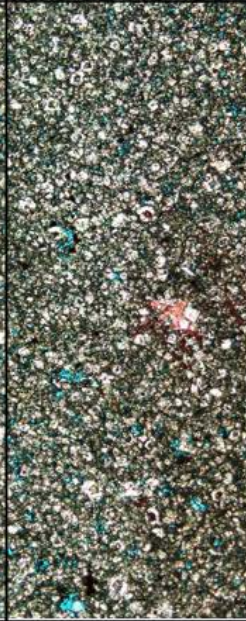
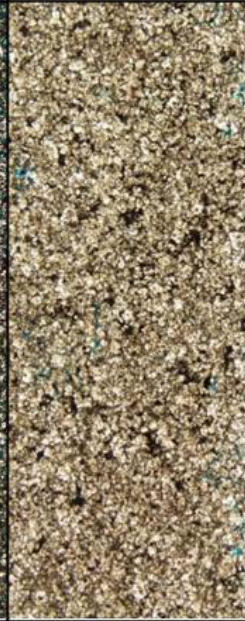

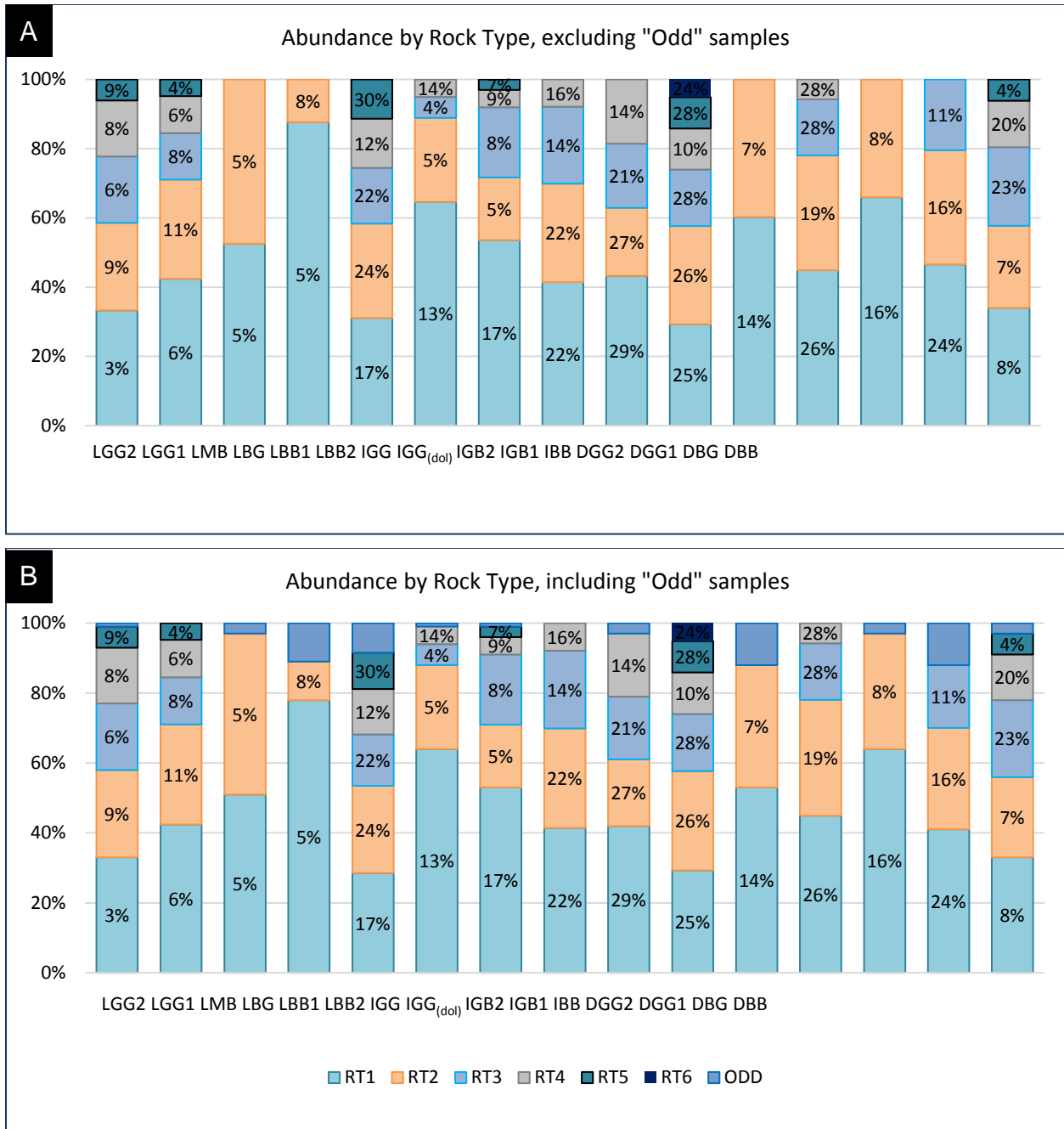
(a)	(b)	(c)	(d)	(e)	(f)	(g)
						
Nonmimetic unimodal planar-s dolomite	Nonmimetic polymodal planar-e dolomite	Nonmimetic polymodal nonplanar dolomite	Nonmimetic unimodal planar-s dolomite	Nonmimetic unimodal planar-s dolomite	Nonmimetic unimodal nonplanar dolomite	Nonmimetic unimodal nonplanar dolomite
DGG2 2° IPI: 8	IGB2 2° IPI: 18	DGG1 2° IPI: 18	IGG 2° IPI: 20	IGB1 2° IPI: 22	DBG 2° IPI: 38	DBB 2° IPI: 44

Figure 12. Dolostone sources under thin section, from low secondary IPI (left) to high secondary IPI (right)

The crystal forms varied from anhedral to euhedral, with some sources exhibiting compromise boundaries (DGG1 and IGB1) and other sources not (IGB2 and IGG [dolostone]). However, in general it can be said that dolostones with low secondary IPI (e.g., DGG2, IGB2, DGG1, IGG [dolostone], IGB1) are fine to coarse grained, are crystal-supported with euhedral to subhedral rhombs, and have porous intercrystalline areas. Conversely, dolostones with high secondary IPI (e.g., DBG and DBB) are very fine-grained and have a tightly interlocking crystal mosaic in subhedral to anhedral form.

### **Helium Porosimetry**

Helium porosimetry revealed that each rock type displayed different porosities, as shown in Figure 13. In the figure, RT1 is the sample with the largest abundance from each source. Note that each RT may differ in characteristics from one source to another.

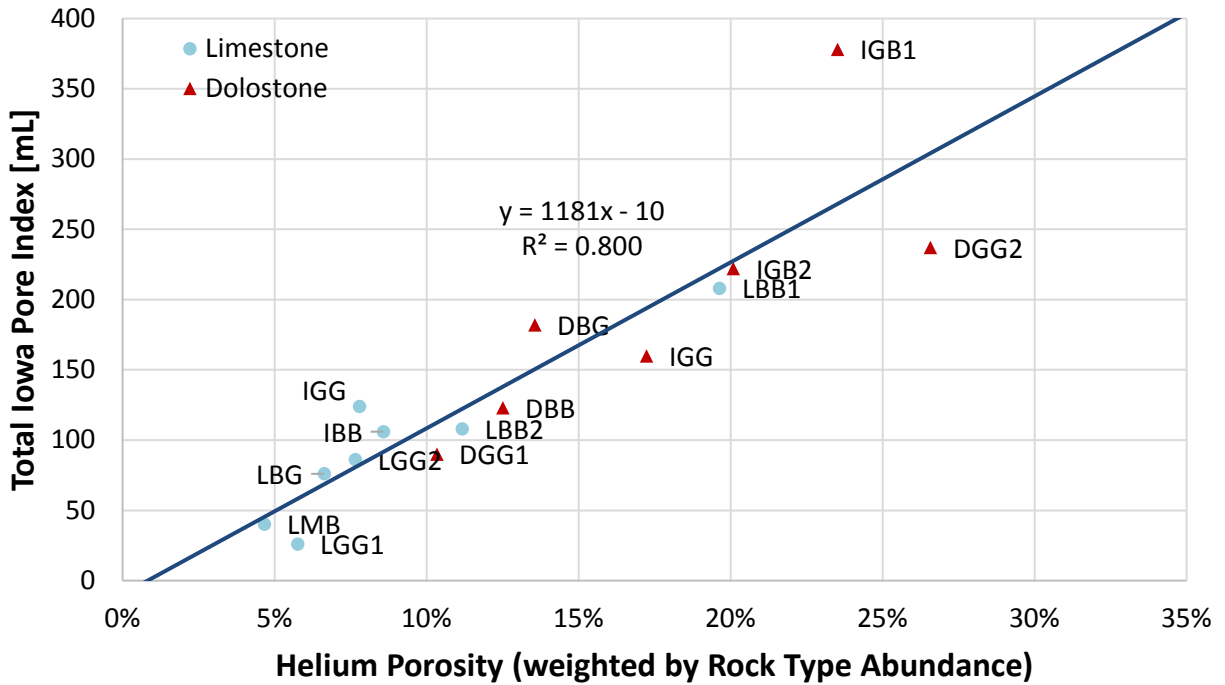


**Figure 13. Different rock types occurring in different abundances and having different porosities**

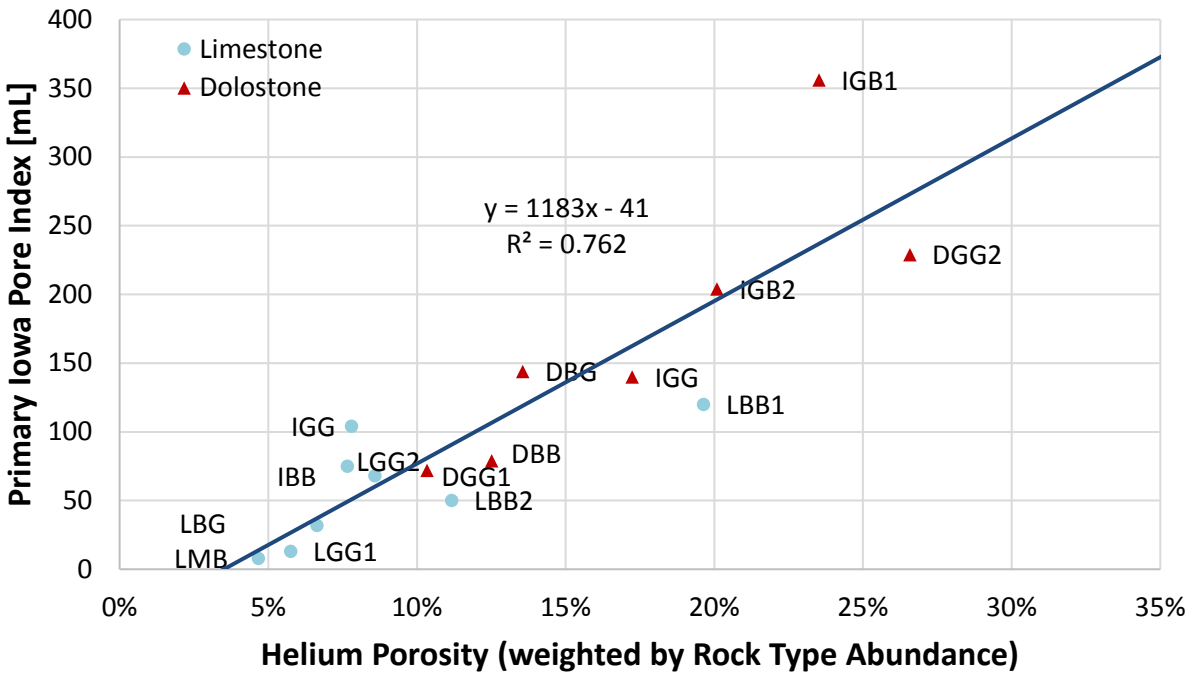
For example, at Alden the least abundant rock type had the lowest porosity (3%), whereas at Osterdock the least abundant rock type had the highest porosity (17%). At Crescent (Upper Hertha) the most abundant rock type had the highest porosity (30%), whereas at Ames Mine the most abundant rock type had the lowest porosity (4%). These differences suggested that it may not be sufficient to test a few pebbles from a source and average the porosities to produce a representative analysis of a sample from the source. Instead, it may be better to weigh the porosities by their rock type abundance to get a bulk porosity representative of the source. This is

because if the few pebbles selected only come from highly porous (or, alternatively, very tight) rock types, then the resultant bulk porosity may be inappropriately skewed.

Helium porosity, weighted by rock type abundance, was found to be linearly correlated with the total IPI (Figure 14) and the primary IPI (Figure 15).



**Figure 14. Positive linear correlation between helium porosity, weighted by rock type abundance, and total pore index, with an  $R^2$  value of 0.80**



**Figure 15. Positive linear correlation between helium porosity, weighted by rock type abundance, and primary pore index, with an  $R^2$  value of 0.76**

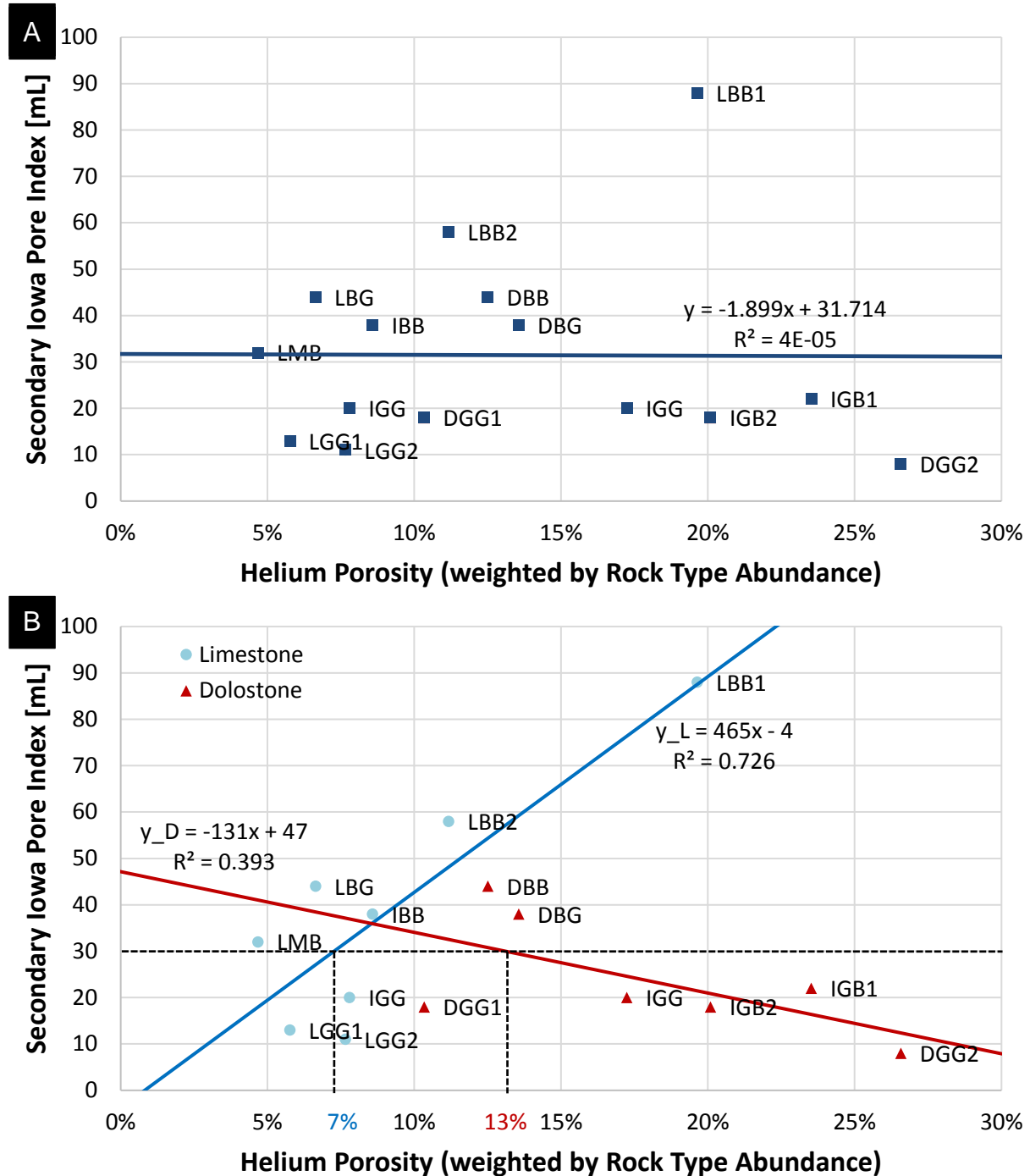
These results were expected because the higher the porosity, the greater the amount of water intrusion into the pore network of the coarse aggregate. The x-intercepts suggested that at 0 mL total IPI the helium porosity was 4%, and at 0 mL primary IPI the helium porosity was 6%. This positive value is likely due to the relatively stronger cohesion among water molecules than among helium atoms. Because liquid water is highly cohesive, it cannot intrude into the smaller pores that are accessible to helium gas. Hence, even with no water intruding into the pores, there may still be porosity in the rock. A zero total IPI does not imply the absence of porosity, but rather the lack of pore-throats (and analysis pressures) large enough to overcome the cohesive forces between the water molecules.

Limestones had lower helium porosity, total IPI, and primary IPI values than dolostones (Figure 15). This can be attributed to the diagenetic process that alter limestones to dolostones (Weyl 1960, Murray 1960, Chilingarian et al. 1992, Warren 2000). When a limestone is exposed to a Mg-rich solution, the denser, smaller-sized Mg ions replace some Ca ions in the mineral structure, hence creating additional porosity in the rock. This causes a higher porosity in dolostones than limestones. Some studies (e.g., Lucia 2004) have also argued that the difference in porosities is actually not due to the formation of dolostones but is instead due to the destruction of porosity in limestones through compaction and cementation. Dolostones tend to have a stronger structure that resists compaction.

An interesting trend was discovered upon inspection of the secondary IPI data. Initially, there seemed to be a very weak correlation between helium porosity and secondary IPI (Figure 16a). However, when lithology was taken into account, the data revealed a strong positive correlation



between helium porosity and secondary IPI for limestones but a weak negative correlation between helium porosity and secondary IPI for dolostones (Figure 16b).

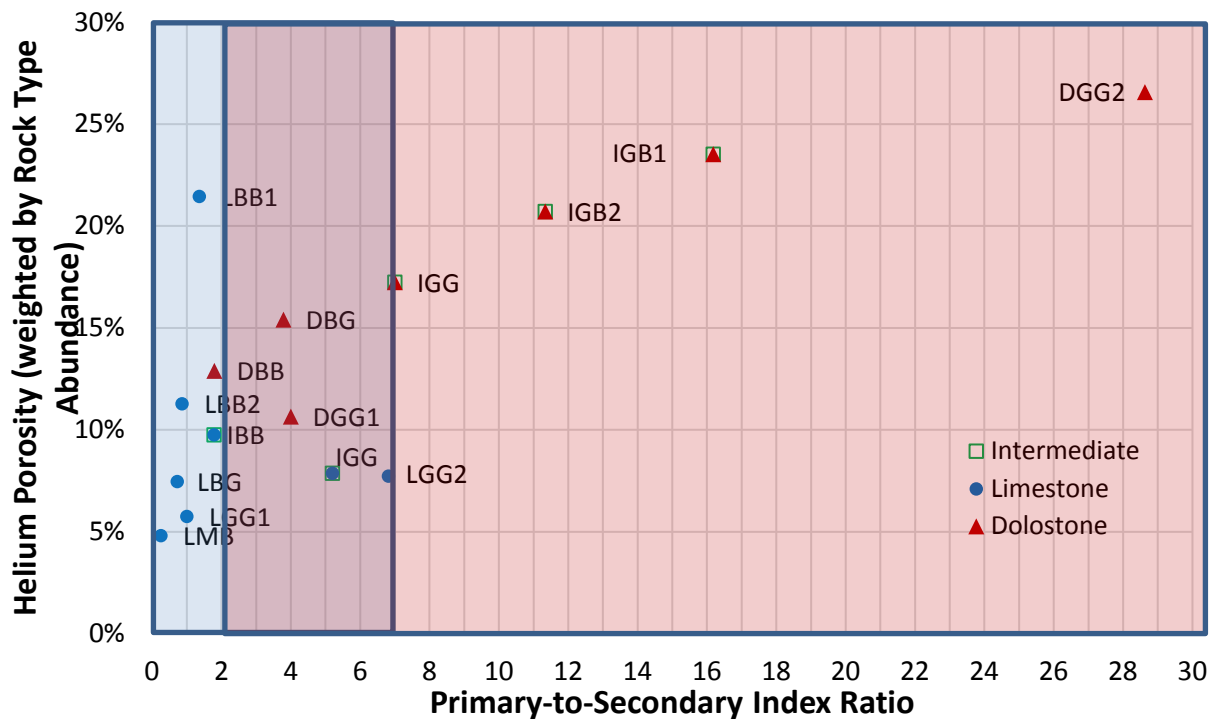


**Figure 16. (a) Poor correlation between between helium porosity, weighted by rock type abundance, and secondary pore index when lithology is ignored as a factor; (b) Positive linear correlation between helium porosity, weighted by rock type abundance, and secondary pore index for limestones and negative linear correlation between helium porosity, weighted by rock type abundance, and secondary pore index for dolostones**



The Iowa DOT specifies that coarse aggregates must have a secondary IPI below 30 mL to pass the lowest durability class rating (Class 2) (Iowa DOT 2003). This corresponds to a helium porosity less than ~7% for limestones and greater than ~13% for dolostones.

To understand the differences in the directions of the linear trends, the ratios of primary to secondary IPI were plotted against helium porosity (Figure 17).



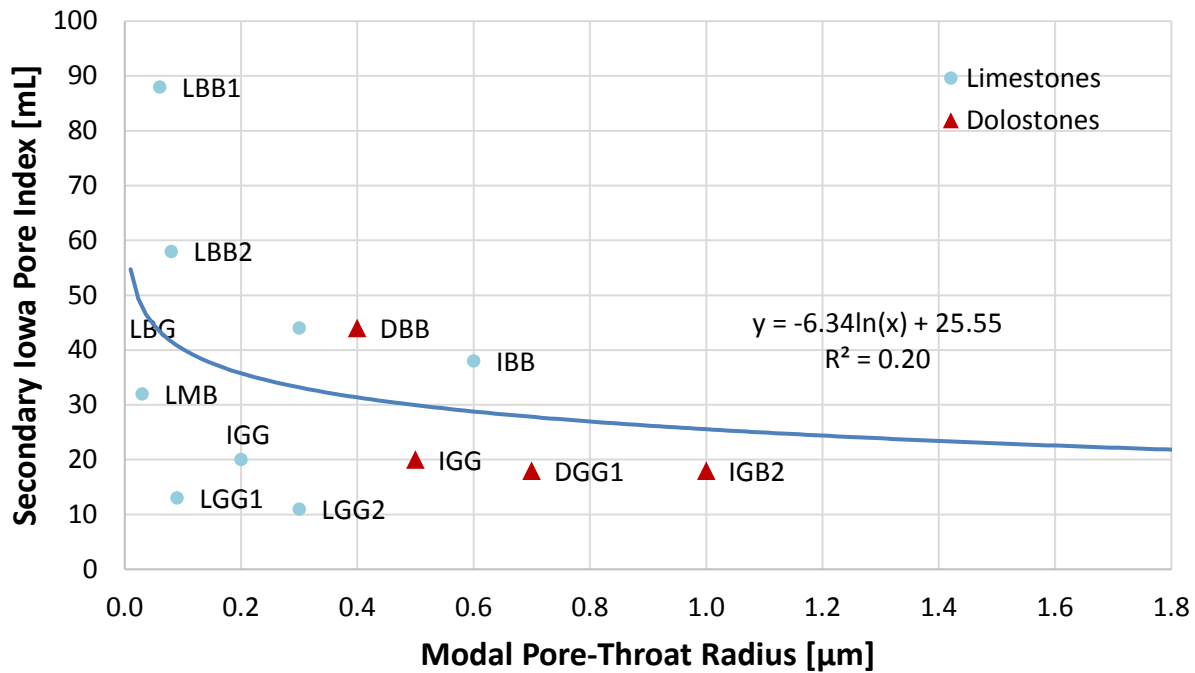
**Figure 17. Primary-to-secondary pore index ratio versus helium porosity**

Limestones generally had a primary-to-secondary IPI ratio of less than 1, while dolostones had a primary-to-secondary IPI ratio of greater than 1. This suggests that the helium porosity in limestones is dominated by the secondary IPI, or micropores, while the helium porosity in dolostones is dominated by the primary IPI, or macropores. The increasing trend in helium porosity and secondary IPI for limestones was observed because a larger proportion of the total porosity can be attributed to the micropores, whereas the opposite trend was observed for dolostones because a larger proportion of the total porosity can be attributed to the macropores.

### Mercury Injection Porosimetry

Mercury injection porosimetry allowed for a more detailed examination of the pore systems of the aggregate sources. While the helium porosimetry data provide a porosity measurement for each source and the IPI data provide a micropore-to-macropore ratio, mercury porosimetry

provides a pore-throat size distribution. Aggregates with low secondary IPI values tended to have large modal pore-throat sizes (Figure 18).



**Figure 18. Large pore-throat diameters yielding low secondary Iowa IPI values**

This finding supports the hypothesis that secondary IPI is a measure of microporosity in a sample. The helium porosimetry results suggested that limestones had lower porosity than dolostones; mercury injection porosimetry suggests that they have smaller modal pore-throat sizes (less than about 0.4 μm) than dolostones (larger than 0.4 μm).

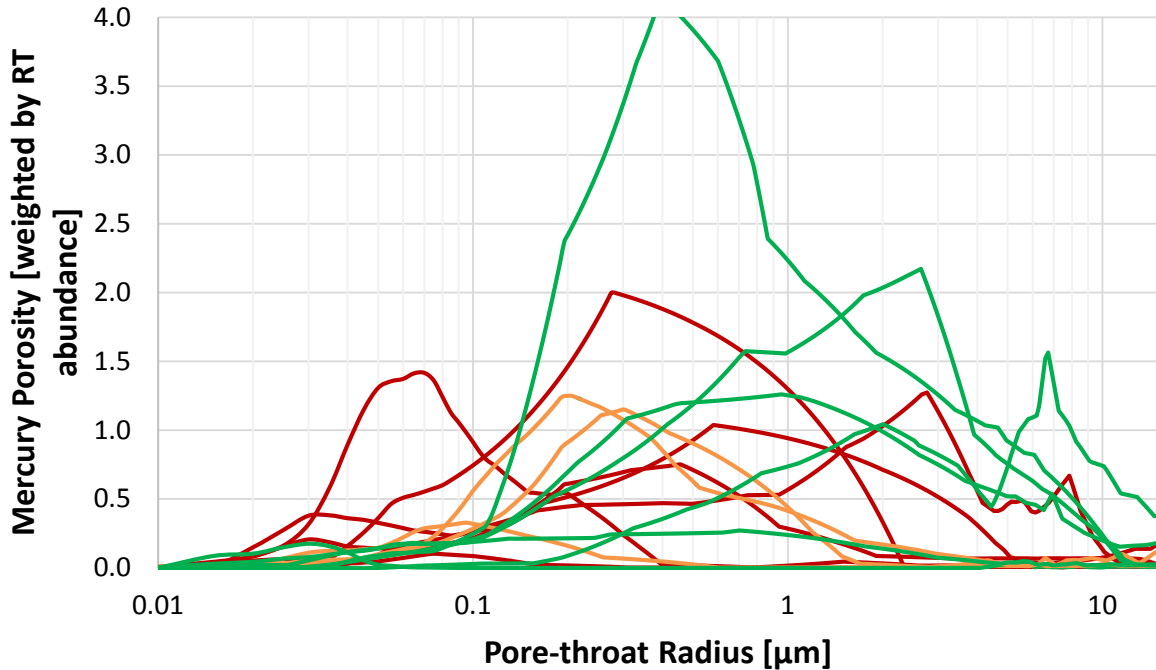
Finding the critical range of pore-throat sizes is important for predicting the performance of aggregates (Walker and Hsieh 1968, Lange and Modry 1969, Koh and Kamada 1973, Litvan 1973, Kaneuji 1978, Shakoor 1982, Marks and Dubberke 1982, Salcedo 1984, Mehta and Monterio 1993). The critical range is defined as the range of pore-throat sizes that enhances aggregate fracturing when the aggregate is exposed to ice segregation mechanisms under steadily subfreezing temperatures. If the pore-throat size is smaller than the critical range, water will have limited access to the pores unless sufficient pressure is applied (FHWA 2015). Even if water has entered the voids, it does not easily freeze due to the high specific surface area of the pores (Everet 1961, Defay et al. 1966, Homshaw 1980). If the pore-throat size is larger than the critical range, water is expelled out of the pores as it freezes, making the aggregate less susceptible to damage (FHWA 2015). Past studies have suggested various critical pore size ranges to characterize aggregates that are susceptible to deterioration, with values ranging from 0.004 to 10 μm (Table 2).

**Table 2. Critical pore-sizes from literature sources**

<b>Source</b>	<b>Critical pore-throat size (<math>\mu\text{m}</math>)</b>	<b>Method of Determination</b>
Sweet 1948	< 5	Petrography
Walker and Hsieh 1968	< 8	Mercury porosimetry
Lange and Modry 1969	0.02 to 0.1	Mercury porosimetry
Koh and Kamada 1973	0.075 to 0.75	Mercury porosimetry
Kaneuji 1978	0.0045 to 1	Mercury porosimetry
Shakoor 1982	0.01 to 10	Mercury porosimetry
Marks and Dubberke 1982	0.04 to 0.2	Mercury porosimetry
Salcedo 1984	0.045 to 10	Mercury porosimetry
Mehta and Monterio 1993	< 1	Mercury porosimetry
Richardson 2009	0.1 to 10	Not mentioned

The critical pore size for Sweet (1948) refers to pore size; the rest refer to pore-throat size.

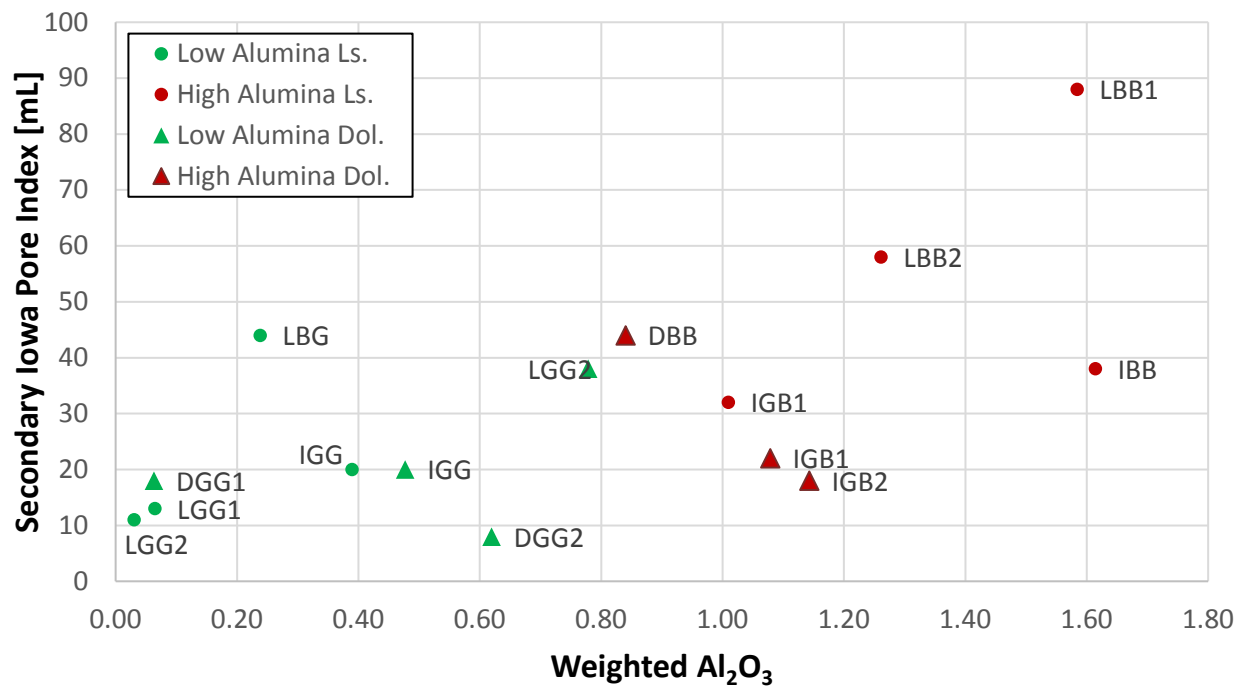
Data on modal pore-throat diameters cannot accurately reveal the range of critical pore sizes responsible for aggregate failure because the modal pore-throat diameter of an aggregate simply indicates the most abundant pore-throat size in the aggregate. It is possible that an aggregate has a modal pore-throat diameter outside the critical range of pore sizes yet still contains enough pores within the critical range to make it susceptible to ice deterioration. This may be expected particularly of dolostone aggregates and aggregates dominated by large pore structures; these rocks are dominated by macropores, yet they are not excepted from the presence and abundance of harmful micropores. What is more relevant, then, is to distinguish a pattern from the pore-throat distribution curves rather than extracting only the modal pore-throat diameter of each aggregate source. Sources in this study with high secondary IPI values dominated the pore-throat range of 0.02 to 0.1  $\mu\text{m}$  (Figure 19).



**Figure 19. Clear trend distinguishing the high (red) and low (green) secondary IPI samples between 0.02 to 0.1 microns, with high secondary IPI samples (>30 mL) shown in red and low secondary IPI samples (<30 mL) shown in green**

### **X-ray Fluorescence**

For this study, XRF data were used not to provide an extensive chemical analysis or interpretation, but to further emphasize the importance of weighting and to verify the extent to which the rock-typing scheme used in this study is reliable. Bulk elemental analyses using XRF data were weighted by rock-type abundance in a similar way to the analyses using helium porosity data. While there was no apparent correlation between alumina content and helium porosity (likely due to a difference in the chemical and mechanical mechanisms of deterioration), there was a clear separation in the alumina data between what the Iowa DOT considers to be high-alumina aggregates and low-alumina aggregates (Figure 20). This separation reaffirmed that the rock-typing scheme used in this study is reliable.



**Figure 20. Separation in alumina data between what the Iowa DOT considers to be high-alumina aggregates and low-alumina aggregates**

## DISCUSSION

The IPI is an attractive method because it estimates the macroporosity-to-microporosity ratio from a relatively significant amount of rock: 4.5 kg, roughly equivalent to 500 to 1,500 pebbles. This should improve the predictive power of the results at the highway scale compared to methods using smaller samples (e.g., core plugs or single pebbles). However, care has to be taken in selecting the proper subsample for subsequent analyses (e.g., XRF, XRD) so the samples are representative of the source.

### Lithology Recategorization

Iowa DOT divides its sources into three lithological categories: limestones, intermediates (mixtures of limestones and dolostones), and dolostones. While some sources were purely calcite or purely dolomite, others contained a mixture of the two. There were no high-Mg calcites or low-Mg dolomites. The intermediate sources were therefore divided into limestone and dolostone categories based on the dominant mineralogy in the sample. The correlation between secondary IPI and helium porosity improved significantly upon reclassification of the aggregate sources and separation of the data by dominant mineralogy, with a correlation coefficient ( $R^2$ ) that went from 0.00004 (treating all sources as having the same lithology) to 0.39 for dolostones and 0.73 for limestones (Figure 16). The following models were derived from analysis of the 15 sources used in this study (IPI is in mL, helium porosity is in volume fraction):

$$\text{Total IPI} = 1181 \times \text{Helium Porosity} - 10 \quad R^2 = 0.80 \quad (2)$$

$$\text{Primary IPI} = 1183 \times \text{Helium Porosity} - 41 \quad R^2 = 0.76 \quad (3)$$

$$\text{Secondary IPI} = 465 \times \text{Helium Porosity} - 4 \quad R^2 = 0.73 \text{ (Limestones)} \quad (4)$$

$$\text{Secondary IPI} = -131 \times \text{Helium Porosity} + 47 \quad R^2 = 0.39 \text{ (Dolostones)} \quad (5)$$

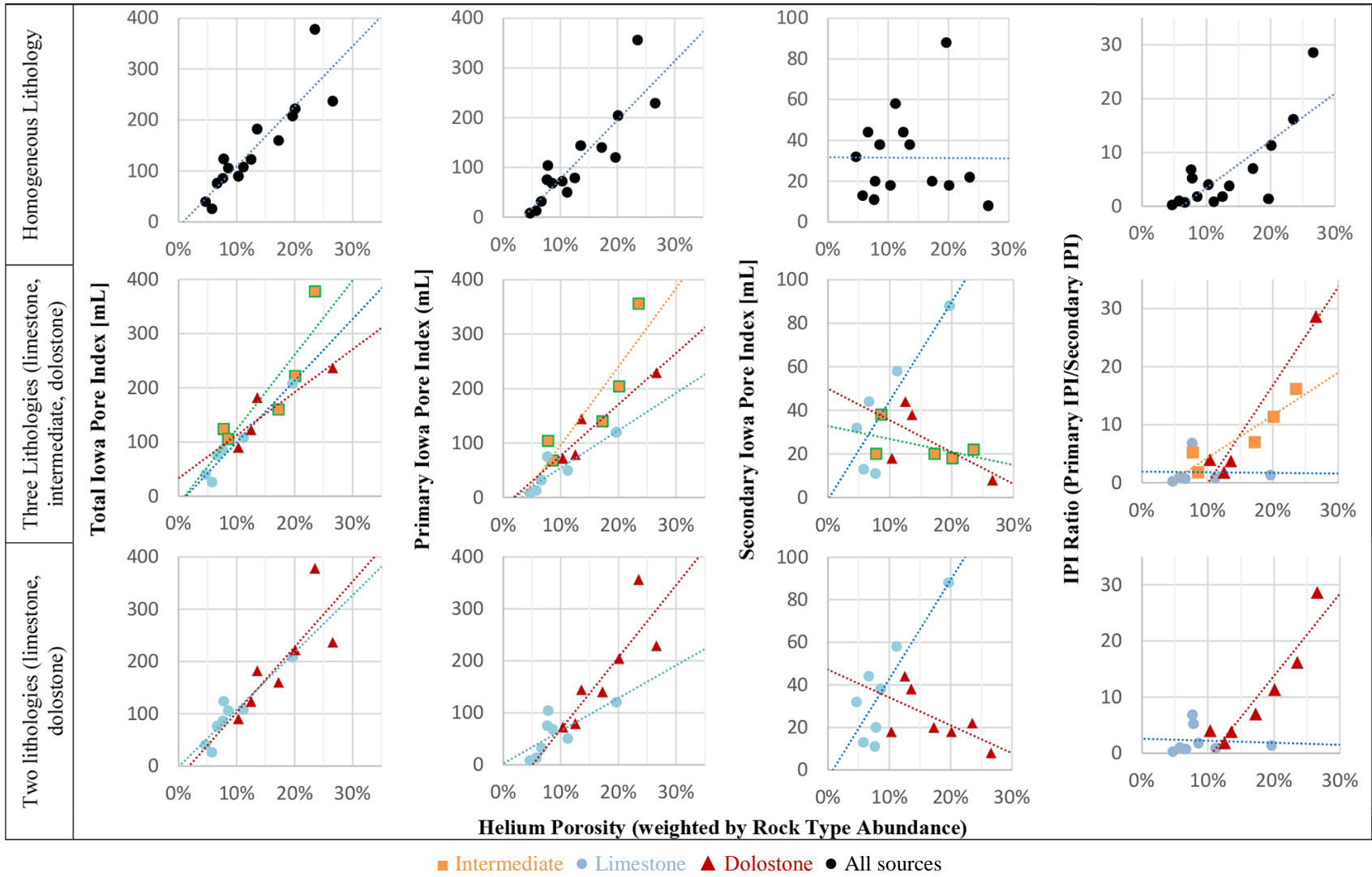
$$\text{IPI Ratio (Primary:Secondary)} = 88 \times \text{Helium Porosity} - 5 \quad R^2 = 0.62 \quad (6)$$

Other possible linear models assuming homogeneous lithology, two lithologies, and three lithologies have also been derived, with the results presented in Table 3.

**Table 3. Helium porosity–IPI transform functions**

<b>Parameter</b>	<b>Group</b>	<b>Lithology/ Category</b>	<b>Slope</b>	<b>Intercept</b>	<b>R<sup>2</sup></b>	<b>Number of Observations</b>
Total IPI	1	All	1181	-10	0.80	15
	2	Limestones	1139	-15	0.95	6
		Intermediates	1377	-15	0.77	5
		Dolostones	794	33	0.80	4
	3	Limestones*	1095	-2	0.85	8
		Dolostones*	1254	-23	0.64	7
1° IPI	1	All	1183	-41	0.76	15
	2	Limestones	685	-14	0.81	6
		Intermediates	1437	-47	0.79	5
		Dolostones	940	-17	0.90	4
	3	Limestones*	630	2	0.54	8
		Dolostones*	1385	-70	0.71	7
2° IPI	1	All	-2	32	0.00004	15
	2	Limestones	454	-1	0.74	6
		Intermediates	-60	33	0.26	5
		Dolostones	-146	50	0.40	4
	3	Limestones*	465	-4	0.73	8
		Dolostones*	-131	47	0.39	7
IPI Ratio (1°/2°)	1	All	88	-5	0.62	15
	2	Limestones	-1	2	0.0006	6
		Intermediates	74	-3	0.85	5
		Dolostones	170	-17	0.95	4
	3	Limestones*	-4	3	0.005	8
		Dolostones*	147	-16	0.87	7

In some cases (e.g., secondary IPI), the R<sup>2</sup> values for three lithologies were higher than the R<sup>2</sup> values for two lithologies. An inspection of the graphs of all parameters (total IPI, primary IPI, secondary IPI, and IPI ratio) showed that the intermediates were widely scattered among limestones and dolostones (Figure 21). However, an obvious pattern can be seen distinguishing limestones from dolostones when only two lithologies were used. This suggests that reclassifying the intermediates as limestones or dolostones might be a simpler scheme than having three lithological categories.



**Figure 21. Helium porosity–IPI by lithology (homogeneous lithology, limestone-intermediate-dolostone, limestone-dolostone)**



These models are significant because they allow primary, secondary, and total IPI to be converted to helium macroporosity, microporosity, and total porosity in an aggregate sample. This allows a direct comparison of IPI, a measurement not widely known outside state departments of transportation, with porosity values reported in the broader geological literature. The Iowa DOT currently has a database of over 5,000 historical IPI analyses.

It should be noted, however, that this reclassification may only be necessary for the conversion of IPI to porosity; it may not be practical and perhaps should be avoided for evaluating the susceptibility of aggregates in the presence of deicing salts. Intermediates are known historically to be poorly correlated with field service records. Dubberke (1989) classified intermediate aggregates as those having a maximum intensity dolomite d-spacing greater than 2.899 Å. While this d-spacing is also characteristic of ankerite, XRF data of our samples showed insufficient iron to suggest the presence of ankerite. Previous experiments (e.g., Dubberke 2002) suggested that the shifted d-spacing is in fact possible in dolomite when Mg ions do not fully replace Ca ions in the lattice structure, as would be expected in pure dolomites. This leads to a lower thermodynamic stability that can be aggravated by the presence of deicing salts. Upon recognition of this phenomenon, the intermediate category should be reintroduced for assessing the stability of the minerals, one of the three factors affecting the durability of aggregates in portland cement concrete (see Source Selection (Sampling Scheme)).

## **Bulk Behavior**

The IPI measures the bulk properties of a coarse aggregate sample, yet, like all petrophysical measurements, it is up to geologists to explain them based on the relative abundance of different rock types in the sample. While each source is treated as a homogenous bulk, the results of sonication, XRF, petrography, and porosimetry reveal that each 4.5 kg sample is a heterogeneous mixture of discrete rock types.

Heterogeneity in rock appearance and pore texture has long been recognized by researchers (e.g., Lemish et al. 1958, Kaneuji 1978, Shakoor 1982, Marks and Dubberke 1982), yet a systematic approach to address this matter has not been developed. Kaneuji (1978) recognized that “when individual pieces were tested, the worst situation showed a spread in total intruded pore volume of about 20%, with a lesser spread in pore diameters.” In sampling the aggregates for experiments, Kaneuji (1978) resorted to using the “blind pick” method, where nine pebbles were selected at random from a pile of crushed and graded aggregates. Shakoor (1982) tested two pieces from each ledge and measured a third sample when necessary to account for any significant differences between the two measurements. The Iowa DOT attempts to account for heterogeneity by practicing ledge control, where evaluations are done on individual beds within a quarry instead of on stockpiles. Unfortunately, recent initiatives by the US Mine Safety and Health Administration to reduce mine worker injuries during such “blockstoning” operations has made it difficult to sample individual beds in a quarry or mine wall. While blockstoning manages to eliminate some variability, there still exists the possibility for beds to grade laterally into other facies.

To rock-type aggregate sources in a geologically appropriate manner, coarse aggregate would need to be categorized based on the following attributes: allochem abundance, allochem type, fossil abundance, fossil type, color, surface texture, and presence of non-carbonate particles (such as glauconite). In this study, however, there was a general lack of variation in allochem and fossil types/abundances within each sample. Therefore, a conservative approach was taken in dividing the rock types based on color, surface texture, and recurrent associations of non-carbonate particles. Subsequent laboratory work largely confirmed that these visual properties separated rock types with measurably different petrographic, geochemical, and petrophysical properties.

This study has shown that the bulk behavior of a sample analyzed by the IPI method is defined by the properties of individual rock types weighted by their abundance in the sample and that the behaviors of the rock types can differ significantly within a source. Currently, XRF chemistry is done by sieving two bags of aggregates and crushing 70 g of 4.8 by 9.5 mm (No. 4 by 3/8 in.) aggregate to a No. 200 mesh size. If a non-representative proportion of rock types is sieved (e.g., if more of the least abundant or odd rock type is selected) to represent a source in subsequent analyses, then the resulting data may not reflect the bulk properties of the sample. This may lead to inaccurate characterization of aggregate quality: a high-quality source may be rejected or a low-quality source may be approved. This point can be demonstrated by our XRF data. For example, in LBB1, RT05 has an  $\text{Al}_2\text{O}_3$  fraction of 0.29 (which is below the threshold value of 0.5), yet the overall weighted  $\text{Al}_2\text{O}_3$  content is 1.58. Conversely, there are also cases where the individual rock types have a higher  $\text{Al}_2\text{O}_3$  content, yet the overall  $\text{Al}_2\text{O}_3$  content is low. For example, in IGG, the  $\text{Al}_2\text{O}_3$  fraction of RT02 and RT04 is 0.65 and 0.60, respectively, yet the overall  $\text{Al}_2\text{O}_3$  is 0.39. Clearly, lithological heterogeneity should be acknowledged in each coarse aggregate sample to avoid costly mischaracterization.

## **Rock Typing**

No single test for accurately predicting the performance of coarse aggregates in pavement roads exposed to ice segregation mechanisms under steadily subfreezing temperatures has the desired attributes of speed and simplicity. While it may not be ideal to separate aggregates first by color, then by surface texture, and then by recurrent associations of non-carbonate particles, this is currently the most practical and rapid way of dividing the aggregates into rock types. We have gone a step further in dividing a seemingly homogeneous source into its multiple rock type constituents.

In distinguishing the rock types, some “odd” samples were discovered. These samples occurred in minimal quantity by weight, less than or equal to 3% oven-dried weight, and were ignored during analysis. The possibility that they may affect pavement performance was not discounted, but further study is needed to assess the extent of any effect they produce.

In other localities, there may be greater visible textural differences, such as a greater diversity of allochems or greater differences in matrix-to-grain ratios, that can be used as criteria to separate rock types. It may also be interesting to compare the results of using different physical attributes and geological histories to categorize the rock types. One such example would be to examine the

petrophysical and chemical behaviors of limestones formed in different depositional environments, including carbonate platforms (e.g., reef carbonates), shoals (oolitic grainstone), lagoons or basins (micrite), and hot springs (travertine).

In the petroleum industry, rock-typing schemes are fairly well-established for dividing subsurface petroleum reservoirs into flow units (e.g., Rushing et al. 2008). This is accomplished by building a geological model that accounts for two factors: (1) the spatial distribution of sediments based on depositional environments and (2) the diagenetic processes (e.g., dolomitization) that affect the sediment post-deposition. The two factors are overlaid to produce a matrix of rock types. A similar scheme was devised to characterize aggregates in this study (Table 4). These rock types can be used to propagate rock properties in a three-dimensional (3D) geological model of a mine or quarry.

**Table 4. Broad depositional environment–diagenesis rock types**

		DEPOSITIONAL ENVIRONMENT			
		Depth	Low Energy		High Energy
<b>DIAGENESIS</b>	<b>Compaction &amp; cementation</b>	Near surface (few 100 m in depth; influenced by local GW flow systems)	Micrite	Peloid	Skeletal
			Muddy		Grainy
	<b>Dissolution &amp; recrystallization</b>		Sparite (meteoric-phreatic zone, source of CaCO <sub>3</sub> : pore fluids; burial, source of CaCO <sub>3</sub> : pressure solution)		
	<b>Replacement</b>		Planar, very fine dolomite	Planar, fine dolomite	Planar, coarse dolomite
		Burial (near surface to >3 km depth; influenced by intermediate to regional GW flow systems (Machel 1999))	Planar, very fine dolomite	Planar, fine dolomite	Planar, coarse dolomite
	Burial (T>50°C) (Woody et al 1996)	Nonplanar, very fine dolomite	Nonplanar, fine dolomite	Nonplanar, coarse dolomite	

Characteristics of low-secondary IPI samples are highlighted in green; characteristics of high-secondary IPI samples are highlighted in red.

Based on petrographic analysis, limestones with low secondary IPI values were interpreted to have formed in shallow, high-energy environments. The peloids, assumed to be fecal pellets, were likely produced by burrowing benthic organisms. The lack of mud also suggested strong water energy that hindered the deposition of fine sediments. The sparite cement indicated a period of diagenesis during which the original sediments were winnowed away, leaving empty pores that were later filled with sparry calcite. Limestones with high secondary IPI values, in

contrast, suggested deposition in deeper, low-energy environments. The abundance of mud and the micrite matrix indicated calm waters in which the fine-grained sediments were deposited.

The depositional environments for dolostones were similar, except that the dolostones had gone through more significant diagenetic alteration. Because crystal sizes in dolostones are dictated by the number of nucleation sites that were available (Scholle and Ulmer-Scholle 2003), coarser-grained dolostones with lower secondary IPI values likely originated from precursor coarse-grained limestones (e.g., skeletal grainstones), while very-fine-grained dolostones with higher secondary IPI values likely originated from precursor fine-grained limestones (e.g., micrite).

### **Critical Pore-Throat Diameters**

Historically, several methods have been used to measure pore-throat distribution, including thin section analysis and mercury porosimetry. The latter has gained widespread recognition as a reliable method and has been used extensively to study the pore networks of cement paste, ceramics, mortar, and aggregates (Walker and Hsieh 1968, Lange and Modry 1969, Koh and Kamada 1973, Kaneuji 1978, Shakoor 1982, Marks and Dubberke 1982, Salcedo 1984, Mehta and Monterio 1993). Previous studies (Table 2) reported mercury data as graphs of cumulative pore volumes versus pore-throat sizes, and a pattern was extracted based on the steepest locations of the slopes where the most intrusion occurred. While some researchers have seen a trend distinguishing good-performing from poor-performing aggregates, others (e.g., Lemish et al. 1958) have failed to do so. Even amongst the former group, there is a wide variability in the reported range of pore-throat sizes responsible for D-cracking, with a lower limit ranging from 0.004 to 0.1  $\mu\text{m}$  and an upper limit ranging from 0.03 to 10  $\mu\text{m}$  (Table 2).

To reconcile these differences, an alternate interpretation of mercury data is offered. Perhaps the more important question to ask is not which pore-throat size is most dominant in an aggregate, but instead whether the aggregate has sufficient pores in the critical range. This is because a sample with an abundance of large pores may still contain an abundance of small pores, even if the relative proportion of the two is greatly different. (As the saying goes, a few bad apples spoil the whole barrel.) A more appropriate representation of the data would therefore be a graph of pore volumes (or porosity) versus pore-throat sizes (Figure 16). A pattern may be extracted based on the relative positions of the curves where poor-performing aggregates are consistently above the good-performing aggregates, suggesting an abundance of harmful porosity in what would be considered the critical range of pore-throat sizes. According to our data, this range is between 0.02 to 0.1  $\mu\text{m}$ .

## CONCLUSIONS

The following discoveries were made in this study based on 15 carbonate sources collected in Iowa:

- *Rock-typing.* Even the most homogenous-appearing sources have at least three different rock types, and each rock type occurs in different abundances and has different porosities. The rock types were originally divided based on physical and textural attributes for convenience but may be subsequently mapped to a depositional environment–diagenesis rock-typing scheme.
- *Petrography.* The intermediates were recategorized into limestones and dolostones based on the dominant mineralogy observed under petrographic examination. This reclassification is only necessary for the conversion of IPI to helium porosity. Limestones with a sparite matrix, peloidal grains, and low matrix-to-allochem ratio (i.e., grainy) have lower secondary IPI values than limestones with a micrite matrix, skeletal grains, and high matrix-to-allochem ratio (i.e., muddy). Dolostones with fine to coarse grains, crystal-supported euhedral to subhedral rhombs, and porous intercrystalline areas have lower secondary IPI values than dolostones with very fine grains and a tightly interlocking crystal mosaic in anhedral form. Aggregates with low secondary IPI values suggested deposition in a shallow, high-energy environment. Aggregates with high secondary IPI values suggested deposition in a deep, low-energy environment.
- *Helium porosimetry.* Several linear models were developed that allow for the conversion of total, primary, and secondary IPI to helium porosity measurements. Limestones with a helium porosity of less than ~7% were found to be desirable for use in road construction. Dolostones with a helium porosity of greater than ~3% were found to be desirable for use in road construction.
- *Mercury porosimetry.* Limestones have modal pore-throat diameters less than about 0.4  $\mu\text{m}$ ; dolostones have modal pore-throat diameters larger than 0.4  $\mu\text{m}$ . While the modal pore-throat diameter is commonly used to differentiate good-performing aggregates from poor-performing aggregates, it is recommended that the pore-throat distributions are examined in total and a pattern is distinguished based on the relative positions of the curves. The critical pore-throat diameter range suggested by this study is between 0.02 to 0.1  $\mu\text{m}$ .

## FURTHER STUDIES

Currently, the IPI operates at constant pressure (35 psi) and reports single primary and secondary IPI values for each sample tested. Helium and mercury porosimetry data revealed that dolostones have a higher porosity and a greater abundance of macroporosity than limestones. Therefore, because the IPI is a time-dependent method, it may be expected that the macroporosity in limestones would fill in more quickly than in dolostones. It is possible that while water is intruding into the larger pores in dolostones, it has already intruded into the smaller pores in limestones given a set amount of time. In terms of the IPI, this suggests that the primary IPI in limestones may actually be a reflection of all macropores and some micropores, or the secondary IPI in dolostones may be a reflection of some macropores and all (or most) micropores. This problem can be addressed either by prolonging the time spent before collecting the primary IPI for aggregates with large volumes of macropores (e.g., dolostones) or by specifying a different secondary IPI cutoff for aggregates with large volumes of macropores than for aggregates with small volumes of macropores (e.g., limestones).

Because the Iowa DOT has already performed over 5,000 IPI analyses, the latter solution is preferred so as to make full use of historical data. To determine an appropriate secondary IPI cutoff, it is recommended that the amount of water intrusion be modeled over time for limestones and dolostones. The slope of the curve generated (i.e., the rate of water intrusion) may be used as an indication of the pore size in the aggregate, where the steeper the slope, the faster the rate and the larger the pore size. The curves of multiple limestone and dolostone aggregates can be compared against each other in a manner similar to how mercury data were analyzed in this study to determine a new secondary IPI cutoff. Once this is established, historical data may be revisited to either accept or reject aggregates.

In this study, emphasis was primarily given to the physical properties of the aggregates. A closer look at the chemistry data may shed some light on the effect of certain minerals or elements on concrete deterioration and the IPI.

It is also recommended that SEM be performed to characterize the nature of  $\mu\text{m}$ - to  $\text{nm}$ -scale porosity. Kaczmarek et al. (2015) identified three main microcrystalline textures: subhedral with large average pore-throat radii ( $\sim 0.7 \mu\text{m}$ ) (Type 1), euhedral and clustered with intermediate average pore-throat radii ( $\sim 0.2 \mu\text{m}$ ) (Type 2), and fitted with small average pore-throat radii ( $\sim 0.06 \mu\text{m}$ ) (Type 3). From these textures, the porosity, permeability, and pore-throat size distribution can be estimated in limestones. Based on the critical pore-throat range suggested by our study, it may be expected that our samples would exhibit microcrystalline textures of Types 2 and 3.

It may also be interesting to compare the results of using industrial computed tomography (CT) scanning against the IPI to obtain the porosity of a 4.5 kg sample. CT is a nondestructive test method that allows petrographic imaging inside a sample without cutting it open. CT would also be able to calculate the bulk volume of an IPI sample of crushed rock. Measuring the bulk volume of such a sample would be unwieldy using the method followed in this paper because it would require analyzing each of the  $\sim 1,000$  pebbles in the sample.

## REFERENCES

- Ahr, W. M. 2008. *Geology of Carbonate Reservoirs: The Identification, Description and Characterization of Hydrocarbon Reservoirs in Carbonate Rocks*. Wiley Publishing, Hoboken, NJ.
- Akagawa, S. and Fukuda, M. 1991. Frost heave mechanism in welded tuff. *Permafrost Periglacial Processes*, Vol. 2, pp. 301–309.
- Al-Tayyib, A. J., Baluch, M. H., Sharif, A. M., and Mahamud, M. M. 1989. The effect of thermal cycling on the durability of concrete made from local materials in the Arabian Gulf countries. *Cement and Concrete Research*, Vol. 19, No. 1, pp. 131–142.
- Chilingarian, G. V., Mazzullo, S. J., and Rieke, H. H. 1992. Carbonate Reservoir Characterization: A Geologic-Engineering Analysis, Part 1. *Developments in Petroleum Geoscience*, Vol. 30.
- Dash, J., Rempel, A., and Wettlaufer, J. 2006. The physics of premelted ice and its geophysical consequences. *Reviews of Modern Physics*, Vol. 78, No. 3, pp. 695–741.
- Davidson, G. P., and Nye, J. F. 1985. A photoelastic study of ice pressure in rock cracks. *Cold Regions Science and Technology*, Vol. 11, No. 2, pp. 141–153.
- Dubberke, W. 2002. *Evaluating Aggregate for PCC; Observations, Comments and Opinion*. <http://www.angelfire.com/ia/concrete/page10.html>. Last accessed October 16, 2017.
- Dubberke, W. and Marks, V. J. 1985. The Effect of Salt on Aggregate Durability. *Transportation Research Record: Journal of the Transportation Research Board*, No. 1031, pp. 27–34.
- Dubberke, W. and Marks, V. J. 1989. *Evaluation of Carbonate Aggregate using X-ray Analysis*. Highway Division, Iowa Department of Transportation, Ames, IA.
- Dunham, R. J. 1962. Classification of Carbonate Rocks according to Depositional Texture. In *Classification of Carbonate Rocks*. American Association of Petroleum Geologists, Tulsa, OK, AAPG Memoir Vol. 1, pp. 108–201.
- Edwards, L., Lubin, M., and Marino, J. 2011. Improving the Repeatability of Coke Bulk Density Testing. In *Light Metals 2011*. Ed. S. J. Lindsay. TMS (The Minerals, Metals & Materials Society). Springer, Cham, Switzerland. pp. 947–952.
- Flügel, E. 2004. *Microfacies of Carbonate Rocks: Analysis, Interpretation and Application*. Springer-Verlag, Berlin-Heidelberg, Germany.
- Folk, R. L. 1959. Practical petrographic classification of limestones. *American Association of Petroleum Geologists Bulletin*, Vol. 43.
- Folk, R. L. 1962. Spectral Subdivision of Limestone Types. In *Classification of Carbonate Rocks*. American Association of Petroleum Geologists, Tulsa, OK, AAPG Memoir Vol. 1, pp. 62–84.
- Ghafoori, N. and Tays, M. W. 2007. Abrasion resistance of early-opening-to-traffic portland cement concrete pavements. *Journal of Materials in Civil Engineering*, Vol. 19, No. 11, pp. 925.
- Gustafson, K., Dawson, R., Jones, K., and Tieck, N. 2015. *Carbonate Rock Pore Size Distribution Determination through Iowa Pore Index Testing*. Iowa Department of Transportation, Ames, IA.
- Hall, K. 1986. Rock moisture content in the field and the laboratory and its relationship to mechanical weathering studies. *Earth Surface Processes and Landforms*. Vol. 11, pp. 131–142.

- Hallet, B. 2006. Geology - Why do freezing rocks break? *Science*, Vol. 314, No. 5802, pp. 1092–1093.
- Iowa DOT. 2003. 4115.04: Aggregate Use Durability Requirements. *Standard Specifications with GS-15005 Revisions*. <https://www.iowadot.gov/erl/current/GS/content/4115.htm>. Last accessed October 16, 2017.
- Iowa DOT. 2015. Level I & II Aggregate Instruction Text: Technical Training and Certification Program, 2015–2016. Iowa Department of Transportation, Ames, IA.
- Iowa DOT. 2016. *General Aggregate Source Information, Materials*. Office of Construction & Materials, Iowa Department of Transportation, Ames, IA.
- Kaneuji, M., Winslow, D. N., and Dolch, W. L. 1980. The relationship between an aggregate's pore size distribution and its freeze thaw durability in concrete. *Cement and Concrete Research*, Vol. 10, No. 2, pp. 433–441.
- Legg Jr., F. E. 1956. Freeze-Thaw Durability of Michigan Concrete Coarse Aggregates. *Transportation Research Record: Journal of the Transportation Research Board*, No. 143, pp. 1–13.
- Lucia, F. 2004. Origin and petrophysics of dolostone pore space. *Geological Society, Special Publications*, Vol. 235, No. 1, pp. 141–155.
- Mehta, P. K. and Montiero, P. J. M. 1993. *Concrete: Structure, Properties, and Materials*. Prentice Hall, Englewood Cliffs, NJ.
- Mohr, B. J. and Bryant, L. B. 2016. Utilization of quarry by-products for reduction of expansion due to alkali-aggregate reaction. *Cement and Concrete Composites*, Vol. 73, pp. 235–240.
- Murray, R. C. 1960. Origin of Porosity in Carbonate Rocks. *Journal of Sedimentary Research*, Society for Sedimentary Geology, Vol. 30.
- Murton, J., Peterson, R., and Ozouf, J. 2006. Bedrock fracture by ice segregation in cold regions. *Science*, Vol. 314, No. 5802, pp. 1127–1129.
- Myers, J. D. and Dubberke, W. 1980. *Iowa Pore Index Test*. Iowa Department of Transportation, Ames, IA.
- Okada, K., Nishibayashi, S., and Kawamura, M. 1989. Alkali-aggregate reaction. *Proceedings of the 8th International Conference*, Kyoto, Japan, July 17–20.
- Owskiak, Z., Zapala-Slaweta, J., and Czapik, P. 2015. Diagnosis of concrete structures distress due to alkali-aggregate reaction. *Bulletin of the Polish Academy Of Sciences-Technical Sciences*, Vol. 63, No. 1, pp. 23–29.
- Rempel, A. 2007. Formation of ice lenses and frost heave. *Journal of Geophysical Research*, Vol. 112, No. F2, F02S21 p.
- Richardson, D. N. 2009. *Quick Test for Durability Factor Estimation*. Missouri University of Science and Technology, Rolla, MO, and Missouri Department of Transportation, Jefferson City, MO.
- Riding, K. A., Blackwell, B., Momeni, A. F., and McLeod, H. 2013. *Effects of Curing Methods and Supplementary Cementitious Material Use on Freeze Thaw Durability of Concrete Containing D-Cracking Aggregates*. Kansas Department of Transportation, Topeka, KS.
- Rushing, J. A., Newsham, K. E., and Blasingame, T. A. 2008. Rock Typing—Keys to understanding productivity in tight gas sands. *SPE 114164*. Society of Petroleum Engineers, Keystone, CO.



- Salcedo, M. A. 1984. *Identification of Frost Susceptible Aggregate and Their Use in Concrete or Bituminous Pavements*. Indiana Department of Transportation and Purdue University, West Lafayette, IN.
- Schauer, F. 1961. Effects of heat and thermal cycling on concrete for reactor shields. MS thesis. Iowa State University, Ames, IA.
- Scherer, G. 1999. Crystallization in pores. *Cement and Concrete Research*, Vol. 29, No. 8, pp. 1347–1358.
- Scholle, P. A. and Ulmer-Scholle, D. S. 2003. *AAPG Memoir 77: A Color Guide to the Petrography of Carbonate Rocks: Grains, Textures, Porosity, Diagenesis*. Ed. J. C. Lorenz. American Association of Petroleum Geologists, Tulsa, OK.
- Shakoor, A., and Scholer, C. F. 1985. Comparison of aggregate pore characteristics as measured by mercury intrusion porosimeter and Iowa pore index tests. *Materials Journal*, American Concrete Institute, Vol. 82, No. 4, pp. 453–458.
- Sibley, D. F. and Gregg, J. M. 1987. Classification of dolomite rock textures. *Journal of Sedimentary Research*, Society for Sedimentary Geology, Vol. 57.
- Sweet, H. 1948. Research on Concrete Durability as Affected by Coarse Aggregate. *Proceedings of ASTM International*, Vol. 48, 988 p.
- Taber, S. 1929. Frost Heaving. *The Journal of Geology*, Vol. 37, No. 5, pp. 428–461.
- Walder, J. and Hallet, B. 1985. A theoretical model of the fracture of rock during freezing. *Geological Society of America Bulletin*, Vol. 96, No. 3, pp. 336–346.
- Walker, R. D. and Hsieh, T. 1968. Relationship between Aggregate Pore Characteristics and Durability of Concrete Exposed to Freezing and Thawing. *Highway Research Record*, No. 226, 41 p.
- Warren, J. 2000. Dolomite: Occurrence, evolution and economically important associations. *Earth Science Reviews*, Vol. 52, No. 1, pp. 1–81.
- Washburn, E. 1921. Note on a Method of Determining the Distribution of Pore Sizes in a Porous Material. *Proceedings of the National Academy of Sciences of the United States of America*, Vol. 7, No. 4, pp. 115-116.
- Weyl, P. K. 1960. Porosity through Dolomitization: Conservation of Mass Requirements. *SEPM Journal of Sedimentary Research*, Society for Sedimentary Geology, Vol. 30.
- Woodson, R. 2009. *Concrete Structures Protection, Repair and Rehabilitation*. Elsevier Science, Burlington, MA.
- Yuan, H., Dangla, P., Chatellier, P., and Chaussadent, T. 2013. Degradation modelling of concrete submitted to sulfuric acid attack. *Cement and Concrete Research*, Vol. 53, pp. 267–277.



## APPENDIX A: HELIUM POROSIMETRY DATA

ID	Operator	OD wt. (g)	AccuPyc		GeoPyc			Iowa Pore Index			Litho-Poro-Chem	Proport-ion with Odds (%)	Proport-ion w/out Odds (%)	Avg Poro of 2 Pebbles	Weighted Poro-sity	Total Weighted Poro-sity
			Vol. (cc)	Density (g/cc)	Vol. (cc)	Density (g/cc)	Poro-sity	Primary (ml)	Sec-on-dary (ml)	Total						
E25-01B	McGee	6.8594	2.5319	2.7092	2.6267	2.6113	3.6%	13	13	26	LGG2	42%	42%	3.7%	1.6%	5.8%
E25-01C	McGee	5.3652	1.9818	2.707	2.0592	2.6052	3.8%	13	13	26						
E25-02A	McGee	6.7136	2.4848	2.7019	2.6209	2.5615	5.2%	13	13	26		29%	29%	5.7%	1.6%	
E25-02B	McGee	7.0406	2.6058	2.7019	2.7765	2.5357	6.1%	13	13	26						
E25-03A	McGee	6.6239	2.4474	2.7065	2.6490	2.5004	7.6%	13	13	26		13%	13%	8.5%	1.1%	
E25-03B	McGee	6.1259	2.2359	2.7398	2.4672	2.4828	9.4%	13	13	26						
E25-04A	McGee	5.7968	2.1509	2.6951	2.4367	2.3789	11.7%	13	13	26		11%	11%	10.8%	1.2%	
E25-04B	McGee	7.0429	2.6071	2.7014	2.8952	2.4325	10.0%	13	13	26						
E25-05A	McGee	5.5092	2.0426	2.6972	2.1398	2.5745	4.5%	13	13	26		5%	5%	5.7%	0.3%	
E25-05B	McGee	5.3066	1.9633	2.7029	2.1069	2.5186	6.8%	13	13	26						
C595-01	Ridzuan	9.1399	3.3897	2.6964	3.7174	2.4587	8.8%	75	11	86	LGG1	33%	33%	8.5%	2.8%	7.7%
C595-01-B	Ridzuan	11.2062	4.1581	2.6950	4.5306	2.4734	8.2%	75	11	86						
C595-02-B	Ridzuan	6.6011	2.4425	2.7026	2.6733	2.4692	8.6%	75	11	86		25%	25%	8.0%	2.0%	
C595-02-C	Ridzuan	7.8183	2.9043	2.6920	3.1364	2.4927	7.4%	75	11	86						
C595-03	Ridzuan	10.0898	3.7421	2.6963	3.9845	2.5323	6.1%	75	11	86		19%	19%	6.2%	1.2%	
C595-03-C	Ridzuan	8.4453	3.1271	2.7007	3.3370	2.5307	6.3%	75	11	86						
C595-04	Ridzuan	10.0170	3.7207	2.6922	4.1163	2.4335	9.6%	75	11	86		16%	16%	9.1%	1.5%	
C595-04-B	Ridzuan	7.0281	2.6121	2.6906	2.8603	2.4570	8.7%	75	11	86						
C595-05-B	Ridzuan	7.2542	2.7101	2.6767	2.8116	2.5801	3.6%	75	11	86		6%	6%	3.3%	0.2%	
C595-05-C	Ridzuan	7.0381	2.6239	2.6823	2.7075	2.5994	3.1%	75	11	86						
E36-01-C	Ridzuan	11.7155	4.3144	2.7155	4.5321	2.5849	4.8%	8	32	40	LMB	51%	53%	5.0%	2.5%	4.7%
E36-01-D	Ridzuan	11.2722	4.1548	2.7131	4.3787	2.5743	5.1%	8	32	40						
E36-02	Ridzuan	9.8582	3.6347	2.7122	3.7882	2.6023	4.1%	8	32	40		46%	47%	4.7%	2.1%	
E36-02-B	Ridzuan	9.1620	3.3697	2.7190	3.5565	2.5760	5.3%	8	32	40						

ID	Operator	OD wt. (g)	AccuPyc		GeoPyc			Iowa Pore Index			Litho-Poro-Chem	Proport-ion with Odds (%)	Proport-ion w/out Odds (%)	Avg Poro of 2 Pebbles	Weight-ed Poro-sity	Total Weight-ed Poro-sity
			Vol. (cc)	Density (g/cc)	Vol. (cc)	Density (g/cc)	Poro-sity	Primary (ml)	Sec-on-dary (ml)	Total						
E43-01	Ridzuan	10.7067	3.9461	2.7132	4.2851	2.4985	7.9%	32	44	76	LBG	78%	88%	7.7%	6.0%	6.6%
E43-01-B	Ridzuan	7.3785	2.7185	2.7142	2.9416	2.5083	7.6%	32	44	76						
E43-02	Ridzuan	7.5811	2.8001	2.7074	2.9673	2.5548	5.6%	32	44	76		11%	12%	5.4%	0.6%	
E43-02-B	Ridzuan	9.2057	3.4012	2.7066	3.5868	2.5665	5.2%	32	44	76						
E33-01	Ridzuan	8.3404	3.0121	2.7690	3.5281	2.3640	14.6%	50	58	108	LBB2	64%	65%	14.3%	9.1%	11.2%
E33-01-B	Ridzuan	10.1022	3.7184	2.7168	4.3215	2.3376	14.0%	50	58	108						
E33-02	Ridzuan	10.7753	3.9750	2.7108	4.1622	2.5889	4.5%	50	58	108		24%	24%	4.3%	1.0%	
E33-02-B	Ridzuan	11.2171	4.1343	2.7132	4.3154	2.5993	4.2%	50	58	108						
E33-03	Ridzuan	11.1668	4.1228	2.7086	4.3566	2.5632	5.4%	50	58	108		6%	6%	5.5%	0.3%	
E33-03-D	Ridzuan	19.1693	7.0853	2.7055	7.5025	2.5550	5.6%	50	58	108						
E33-04-U	Ridzuan	13.7575	5.0749	2.7109	5.9566	2.3095	14.8%	50	58	108		5%	5%	13.1%	0.7%	
E33-04-B	Ridzuan	11.1377	4.0552	2.7465	4.5722	2.4359	11.3%	50	58	108						
E-45-1A	McGee	9.1942	3.3052	2.7817	4.6654	1.9707	29.15%	120	88	208	LBB1	29%	31%	29.7%	8.5%	19.6%
E-45-1C	McGee	8.6542	3.1106	2.7821	4.4656	1.9379	30.34%	120	88	208						
E-45-2A	McGee	9.4503	3.4756	2.719	4.0040	2.3601	13.20%	120	88	208		25%	27%	12.4%	3.1%	
E-45-2C	McGee	7.393	2.7090	2.729	3.0625	2.4140	11.54%	120	88	208						
E-45-3A	McGee	5.8583	2.1431	2.7335	2.6789	2.1970	23.68%	120	88	208		15%	16%	22.1%	3.2%	
E-45-3C	McGee	9.3953	3.3522	2.8027	4.2133	2.2298	20.44%	120	88	208						
E-45-4A	McGee	8.4081	3.0873	2.7235	4.0558	2.0730	23.88%	120	88	208		13%	14%	23.9%	3.1%	
E-45-4C	McGee	9.3792	3.4201	2.7423	4.4929	2.0875	23.88%	120	88	208						
E-45-5A	McGee	6.936	2.5234	2.7487	3.0374	2.2835	16.92%	120	88	208		10%	11%	16.6%	1.7%	
E-45-5B	McGee	6.0288	2.1944	2.7474	2.6219	2.2990	16.31%	120	88	208						
E47-1A-B	Ridzuan	12.0322	4.3512	2.7652	4.7217	2.5482	7.8%	104	20	124	IGG	53%	54%	7.0%	3.7%	7.8%
E47-1A-C	Ridzuan	7.5377	2.6614	2.8322	2.8367	2.6571	6.2%	104	20	124						
E47-1B	Ridzuan	10.6791	3.7675	2.8345	4.1404	2.5793	9.0%	104	20	124		18%	18%	9.2%	1.7%	
E47-1B-C	Ridzuan	7.8056	2.7619	2.8261	3.0486	2.5603	9.4%	104	20	124						
E47-02	Ridzuan	8.9604	3.2594	2.7491	3.5076	2.5546	7.1%	104	20	124		20%	20%	8.3%	1.7%	

ID	Operator	OD wt. (g)	AccuPyc		GeoPyc			Iowa Pore Index			Litho-Poro-Chem	Proportion with Odds (%)	Proportion w/out Odds (%)	Avg Poro of 2 Pebbles	Weighted Porosity	Total Weighted Porosity
			Vol. (cc)	Density (g/cc)	Vol. (cc)	Density (g/cc)	Porosity	Primary (ml)	Secondary (ml)	Total						
E47-02-B	Ridzuan	8.4985	3.0171	2.8167	3.3312	2.5511	9.4%	104	20	124						
E47-03	Ridzuan	7.5991	2.7261	2.7875	2.8547	2.6619	4.5%	104	20	124		5%	5%	5.0%	0.2%	
E47-03-C	Ridzuan	7.4133	2.6728	2.7736	2.8263	2.6229	5.4%	104	20	124						
E47-04-U	Ridzuan	5.5006	1.9207	2.8639	2.3593	2.3314	18.6%	104	20	124		3%	3%	17.4%	0.5%	
E47-04-B	Ridzuan	3.3934	1.1937	2.8427	1.4256	2.3803	16.3%	104	20	124						
E41-1A	McGee	8.9329	3.1436	2.8416	4.1516	2.1516	24.3%	356	22	378	IGB1	29%	29%	24.1%	7.0%	23.5%
E41-1A-C	McGee	6.6334	2.3397	2.8351	3.0738	2.1580	23.9%	356	22	378						
E41-1B	McGee	10.175	3.5889	2.8351	4.9774	2.0442	27.9%	356	22	378		28%	28%	27.5%	7.8%	
E41-1B-B	McGee	9.9324	3.4951	2.8418	4.77973	2.0703	27.1%	356	22	378						
E41-2A	McGee	10.9101	4.0321	2.7058	4.4593	2.4465	9.6%	356	22	378		16%	16%	10.3%	1.7%	
E41-2A-B	McGee	13.2782	4.8853	2.7180	5.4858	2.4204	10.9%	356	22	378						
E41-2B	McGee	7.7184	2.7058	2.8525	3.6304	2.1260	25.5%	356	22	378		12%	12%	28.3%	3.4%	
E41-2B-C	McGee	9.2984	3.2648	2.8480	4.7432	1.9603	31.2%	356	22	378						
E41-3A	McGee	9.8480	3.4952	2.8176	4.7273	2.0831	26.1%	356	22	378		9%	9%	26.0%	2.3%	
E41-3A-C	McGee	8.2961	2.9194	2.8417	3.9464	2.1021	26.0%	356	22	378						
E41-3B	McGee	11.4849	4.0284	2.8510	5.3222	2.1579	24.3%	356	22	378		5%	5%	25.0%	1.3%	
E41-3B-B	McGee	12.9996	4.5703	2.8444	6.1445	2.1156	25.6%	356	22	378						
E35-01-C	Ridzuan	8.9242	3.1341	2.8475	3.6803	2.4248	14.8%	204	18	222	IGB2	42%	43%	14.2%	6.0%	20.1%
E35-01-D	Ridzuan	7.5375	2.6591	2.8346	3.0796	2.4475	13.7%	204	18	222						
E35-2A	Ridzuan	8.8824	3.1416	2.8273	4.0161	2.2117	21.8%	204	18	222		19%	20%	20.7%	3.9%	
E35-2A-B	Ridzuan	5.0672	1.7589	2.8809	2.1907	2.3129	19.7%	204	18	222						
E35-2B	Ridzuan	8.7394	3.0462	2.8690	4.0894	2.1371	25.5%	204	18	222		18%	19%	27.1%	4.9%	
E35-2B-D	Ridzuan	8.1155	2.8445	2.8531	3.9882	2.0348	28.7%	204	18	222						
E35-2C	Ridzuan	6.5372	2.2894	2.8554	3.3136	1.9728	30.9%	204	18	222		18%	19%	29.4%	5.3%	
E35-2C-B	Ridzuan	5.7937	2.0269	2.8584	2.8096	2.0620	27.9%	204	18	222						
B36-01	McGee	8.8898	3.1318	2.8286	3.7353	2.3799	15.9%	140	20	160	IGG <sub>dol</sub>	41%	41%	16.3%	6.7%	17.2%
B36-01-B	McGee	5.5965	1.9797	2.8269	2.3758	2.3556	16.7%	140	20	160						

ID	Operator	OD wt. (g)	AccuPyc		GeoPyc			Iowa Pore Index			Litho-Poro-Chem	Proport-ion with Odds (%)	Proport-ion w/out Odds (%)	Avg Poro of 2 Pebbles	Weight-ed Poro-sity	Total Weight-ed Poro-sity
			Vol. (cc)	Density (g/cc)	Vol. (cc)	Density (g/cc)	Poro-sity	Primary (ml)	Sec-on-dary (ml)	Total						
B36-02-B	McGee	8.4339	3.0365	2.7775	3.5253	2.3923	13.9%	140	20	160		28%	28%	13.6%	3.9%	
B36-02-C	McGee	4.4038	1.5856	2.7774	1.8280	2.4090	13.3%	140	20	160						
B36-03	McGee	7.2283	2.5362	2.8501	3.4439	2.0988	26.4%	140	20	160		22%	22%	22.2%	5.0%	
B36-03-B	McGee	6.5437	2.3396	2.7970	2.8568	2.2905	18.1%	140	20	160						
B36-04	McGee	7.5815	2.6733	2.8360	3.5126	2.1583	23.9%	140	20	160		8%	8%	21.5%	1.7%	
B36-04-B	McGee	4.4900	1.5924	2.8197	1.9693	2.2799	19.1%	140	20	160						
B27-01	Ridzuan	9.4418	3.3937	2.7821	3.6165	2.6107	6.2%	68	38	106	IBB	53%	60%	6.8%	3.6%	8.6%
B27-01-C	Ridzuan	8.7102	3.1790	2.7399	3.4315	2.5382	7.4%	68	38	106						
B27-02	Ridzuan	10.4920	3.6863	2.8462	4.2286	2.4812	12.8%	68	38	106		35%	40%	14.3%	5.0%	
B27-02-B	Ridzuan	8.0788	2.8214	2.8634	3.3481	2.4129	15.7%	68	38	106						
E58-01	McGee	8.8803	3.1193	2.8469	4.3633	2.0352	28.5%	229	8	237	DGG2	45%	45%	28.3%	12.7%	26.6%
E58-01-B	McGee	4.5057	1.5984	2.8189	2.2256	2.0244	28.2%	229	8	237						
E58-02	McGee	8.1734	2.8816	2.8364	3.9912	2.0478	27.8%	229	8	237		33%	33%	27.9%	9.2%	
E58-02-B	McGee	4.0936	1.4473	2.8285	2.0091	2.0374	28.0%	229	8	237						
E58-03	McGee	7.9203	2.8470	2.7820	3.3474	2.1670	23.8%	229	8	237		16%	16%	19.2%	3.1%	
E58-03-B	McGee	9.2846	3.2819	2.8290	3.8435	2.4156	14.6%	229	8	237						
E58-04	McGee	7.2540	2.5510	2.8436	3.3474	2.1670	23.8%	229	8	237		6%	6%	25.9%	1.5%	
E58-04-C	McGee	4.0443	1.4349	2.8185	1.9955	2.0266	28.1%	229	8	237						
E61-01	Ridzuan	9.2633	3.2689	2.8338	3.5545	2.6060	8.0%	72	18	90	DGG1	64%	66%	7.9%	5.0%	10.3%
E61-01-C	Ridzuan	7.6134	2.7098	2.8096	2.9357	2.5933	7.7%	72	18	90						
E61-02-U	Ridzuan	8.8645	3.1266	2.8352	3.6649	2.4187	14.7%	72	18	90		33%	34%	16.1%	5.3%	
E61-02-B	Ridzuan	7.7065	2.7300	2.8229	3.3067	2.3305	17.4%	72	18	90						
E42-01-B	Ridzuan	11.3535	3.9817	2.8514	4.5210	2.5113	11.9%	144	38	182	DBG	41%	47%	11.3%	4.6%	13.6%
E42-01-C	Ridzuan	7.3808	2.6120	2.8258	2.9216	2.5262	10.6%	144	38	182						
E42-02	Ridzuan	8.8343	3.1082	2.8423	3.7147	2.3782	16.3%	144	38	182		29%	33%	15.8%	4.6%	
E42-02-C	Ridzuan	6.0532	2.1323	2.8388	2.5173	2.4046	15.3%	144	38	182						
E42-03	Ridzuan	7.8935	2.7766	2.8428	3.7087	2.1284	25.1%	144	38	182		18%	20%	24.2%	4.4%	

ID	Operator	OD wt. (g)	AccuPyc		GeoPyc			Iowa Pore Index			Litho-Poro-Chem	Proport-ion with Odds (%)	Proport-ion w/out Odds (%)	Avg Poro of 2 Pebbles	Weight-ed Poro-sity	Total Weight-ed Poro-sity
			Vol. (cc)	Density (g/cc)	Vol. (cc)	Density (g/cc)	Poro-sity	Primary (ml)	Sec-on-dary (ml)	Total						
E42-03-B	Ridzuan	6.2957	2.2124	2.8456	2.8822	2.1843	23.2%	144	38	182						
E52-01-C	Ridzuan	10.1663	3.6127	2.8141	3.7897	2.6826	4.7%	79	44	123	DBB	33%	34%	4.3%	1.4%	12.5%
E52-01-D	Ridzuan	8.7155	3.0911	2.8196	3.2174	2.7088	3.9%	79	44	123						
E52-02-B	Ridzuan	9.0738	3.1999	2.8357	4.0188	2.2578	20.4%	79	44	123		23%	24%	20.3%	4.7%	
E52-02-C	Ridzuan	10.7741	3.8129	2.8257	4.7835	2.2523	20.3%	79	44	123						
E52-03	Ridzuan	8.7429	3.0695	2.8484	4.0489	2.1593	24.2%	79	44	123		22%	23%	22.6%	5.0%	
E52-03-C	Ridzuan	8.5866	3.0032	2.8591	3.8051	2.2562	21.1%	79	44	123						
E52-04	Ridzuan	10.0189	3.5367	2.8328	3.7997	2.6367	6.9%	79	44	123		13%	13%	7.2%	0.9%	
E52-04-C	Ridzuan	7.2546	2.5608	2.8330	2.7650	2.6237	7.4%	79	44	123						
E52-05	Ridzuan	9.4999	3.4051	2.7899	3.6853	2.5778	7.6%	79	44	123		6%	6%	8.4%	0.5%	
E52-05-B	Ridzuan	7.3766	2.6164	2.8194	2.8809	2.5605	9.2%	79	44	123						





## APPENDIX B: XRF DATA

Seq.	Meas. date/time	Sample ID	Sum of conc (%)	Proportion (%)	Porportion 2 (%)	CaO	MgO	SiO <sub>2</sub>	Al <sub>2</sub> O <sub>3</sub>	K <sub>2</sub> O	Fe <sub>2</sub> O <sub>3</sub>	TiO <sub>2</sub>	Cl	S	Na <sub>2</sub> O	P <sub>2</sub> O <sub>5</sub>	MnO	SrO	Zn	Cr	Ba	
						Ca	Mg	Si	Al	K	Fe	Ti	Cl	S	Na	P	Mn	Sr	Zn	Cr	Ba	
						(%)	(%)	(%)	(%)	(%)	(%)	(%)	(%)	(%)	(%)	(%)	(%)	(%)	(%)	(%)	(%)	(%)
LGG1	5	8/10/2016 8:12	E25-01A	52.2	42	42	54.6	0.3	0.3	0.11	0.0	0.2	0.0	0.0	0.1	0.0	0.0	0.0	0.0	0.0	0.0	0.0
LGG1	6	8/10/2016 8:19	E25-02A	55.7	29	29	55.2	0.2	0.0	0.02	0.0	0.1	0.0	0.0	0.0	0.0	0.0	0.0	0.0	0.0	0.0	0.0
LGG1	7	8/10/2016 8:27	E25-03B	57.0	13	13	53.7	0.4	0.0	0.02	0.0	1.6	0.0	0.0	0.6	0.5	0.0	0.0	0.0	0.0	0.0	0.0
LGG1	8	8/10/2016 8:34	E25-04A	54.4	11	11	53.9	0.3	0.0	0.01	0.0	0.1	0.0	0.0	0.0	0.0	0.0	0.0	0.0	0.0	0.0	0.0
LGG1	9	8/10/2016 8:42	E25-05B	55.9	5	5	53.8	0.3	0.6	0.22	0.1	0.6	0.0	0.0	0.2	0.0	0.0	0.0	0.0	0.0	0.0	0.0
LGG2	28	4/6/2016	AAC595-01	55.9	33	33	55.3	0.2	0.1	0.02	0.0	0.1	0.0	0.0	0.0	0.0	0.0	0.0	0.0	0.0	0.0	0.0
LGG2	29	4/6/2016	AAC595-02B	55.7	25	25	54.7	0.2	0.1	0.02	0.0	0.4	0.0	0.0	0.2	0.0	0.0	0.0	0.0	0.0	0.0	0.0
LGG2	30	4/6/2016	AAC595-03C	55.0	19	19	53.8	0.2	0.1	0.06	0.0	0.4	0.0	0.0	0.1	0.0	0.0	0.0	0.0	0.0	0.0	0.0
LGG2	31	4/6/2016	AAC595-04B	55.4	16	16	54.5	0.3	0.1	0.03	0.0	0.3	0.0	0.0	0.0	0.0	0.0	0.0	0.0	0.0	0.0	0.0
LGG2	32	4/6/2016	AAC595-05C	55.6	6	6	54.7	0.4	0.1	0.04	0.0	0.2	0.0	0.0	0.0	0.0	0.0	0.0	0.0	0.0	0.0	0.0
LMB	26	4/6/2016	AAE36-01C	60.0	51	53	48.6	0.6	8.2	1.24	0.4	0.6	0.1	0.0	0.1	0.0	0.1	0.1	0.0	0.0	0.0	0.0
LMB	27	4/6/2016	AAE36-02B	57.8	46	47	51.4	0.4	4.2	0.75	0.2	0.4	0.0	0.0	0.1	0.0	0.0	0.1	0.0	0.0	0.0	0.0
LBG	24	4/6/2016	AAE43-01B	56.5	78	88	52.8	0.5	2.4	0.24	0.1	0.3	0.0	0.0	0.1	0.0	0.0	0.0	0.1	0.0	0.0	0.0
LBG	25	4/6/2016	AAE43-02	56.6	11	12	54.1	0.5	1.3	0.21	0.0	0.2	0.0	0.0	0.0	0.0	0.0	0.0	0.1	0.0	0.0	0.0
LBB1	16	8/10/2016 9:35	E45-01A	68.6	29	31	17.3	5.6	39.4	3.07	0.8	1.4	0.1	0.0	0.3	0.2	0.2	0.0	0.1	0.0	0.0	0.0
LBB1	17	8/10/2016 9:43	E45-02B	59.0	25	27	45.7	1.3	10.2	0.47	0.1	0.7	0.0	0.0	0.1	0.0	0.0	0.1	0.1	0.0	0.0	0.0
LBB1	18	8/10/2016 9:50	E45-03C	60.8	15	16	32.8	7.1	16.8	2.09	0.5	1.1	0.1	0.0	0.2	0.1	0.0	0.1	0.1	0.0	0.0	0.0
LBB1	19	8/10/2016 9:58	E45-04A	67.4	13	14	21.9	2.5	40.8	0.93	0.2	0.6	0.0	0.0	0.1	0.1	0.1	0.0	0.0	0.0	0.0	0.0

Seq.	Meas. date/time	Sample ID	Sum of conc (%)	Proportion (%)	Porportion 2 (%)	CaO	MgO	SiO <sub>2</sub>	Al <sub>2</sub> O <sub>3</sub>	K <sub>2</sub> O	Fe <sub>2</sub> O <sub>3</sub>	TiO <sub>2</sub>	Cl	S	Na <sub>2</sub> O	P <sub>2</sub> O <sub>5</sub>	MnO	SrO	Zn	Cr	Ba	
						Ca	Mg	Si	Al	K	Fe	Ti	Cl	S	Na	P	Mn	Sr	Zn	Cr	Ba	
						(%)	(%)	(%)	(%)	(%)	(%)	(%)	(%)	(%)	(%)	(%)	(%)	(%)	(%)	(%)	(%)	(%)
LBB1	20	8/10/2016 10:05	E45-05C	56.7	10	11	49.3	1.3	4.9	0.29	0.1	0.6	0.0	0.0	0.1	0.0	0.0	0.1	0.1	0.0	0.0	0.0
LBB2	16	4/6/2016	AAE33-01	62.3	64	65	41.4	1.2	16.4	1.64	0.4	0.8	0.1	0.0	0.1	0.1	0.0	0.0	0.1	0.0	0.0	0.0
LBB2	17	4/6/2016	AAE33-02	56.9	24	24	52.0	0.6	3.1	0.42	0.1	0.3	0.0	0.0	0.0	0.1	0.0	0.0	0.1	0.0	0.0	0.0
LBB2	18	4/6/2016	AAE33-03	56.7	6	6	50.1	0.6	5.0	0.36	0.1	0.3	0.0	0.0	0.0	0.0	0.0	0.1	0.1	0.0	0.0	0.0
LBB2	19	4/6/2016	AAE33-04	63.4	5	5	41.4	1.4	17.4	1.51	0.4	0.8	0.1	0.0	0.2	0.2	0.1	0.0	0.1	0.0	0.0	0.0
IGG	6	4/6/2016	AAE47-1AC	54.7	53	54	31.8	19.5	2.0	0.38	0.2	0.6	0.0	0.0	0.0	0.0	0.0	0.1	0.0	0.0	0.0	0.0
IGG	7	4/6/2016	AAE47-1BC	55.5	18	18	30.0	20.3	3.3	0.65	0.4	0.6	0.0	0.1	0.0	0.1	0.1	0.0	0.0	0.0	0.0	0.0
IGG	8	4/6/2016	AAE47-02	54.0	20	20	48.1	4.3	1.1	0.13	0.1	0.2	0.0	0.0	0.0	0.0	0.0	0.0	0.0	0.0	0.0	0.0
IGG	9	4/6/2016	AAE47-03	55.1	5	5	38.9	11.6	3.0	0.60	0.3	0.4	0.0	0.0	0.0	0.0	0.0	0.0	0.0	0.0	0.0	0.0
IGG	10	4/6/2016	AAE47-04B	54.0	3	3	29.9	20.8	1.8	0.34	0.2	0.7	0.0	0.1	0.0	0.0	0.0	0.1	0.0	0.0	0.0	0.0
IGB1	10	8/10/2016 8:50	E41-1AA	59.3	29	29	30.9	17.1	7.9	1.31	0.7	1.0	0.1	0.0	0.1	0.1	0.1	0.1	0.0	0.0	0.0	0.0
IGB1	11	8/10/2016 8:57	E41-1BB	59.0	28	28	30.9	17.3	7.5	1.34	0.7	0.9	0.1	0.0	0.1	0.0	0.0	0.1	0.0	0.0	0.0	0.0
IGB1	12	8/10/2016 9:05	E41-2AC	57.6	16	16	49.9	2.4	3.7	0.46	0.3	0.4	0.0	0.0	0.0	0.2	0.1	0.0	0.0	0.0	0.0	0.0
IGB1	13	8/10/2016 9:12	E41-2BA	52.6	12	12	33.3	18.2	0.6	0.11	0.1	0.1	0.0	0.0	0.0	0.0	0.0	0.0	0.0	0.0	0.0	0.0
IGB1	14	8/10/2016 9:20	E41-3AB	59.9	9	9	31.4	15.0	9.5	1.59	0.9	1.3	0.1	0.0	0.1	0.0	0.0	0.1	0.0	0.0	0.0	0.0
IGB1	15	8/10/2016 9:27	E41-3BB	60.2	5	5	31.0	16.5	9.1	1.62	0.8	0.8	0.1	0.0	0.1	0.0	0.1	0.1	0.0	0.0	0.0	0.0
CBJ	20	4/6/2016	AAE35-01D	54.9	42	43	31.5	18.6	2.8	0.56	0.2	0.8	0.0	0.0	0.2	0.1	0.0	0.1	0.0	0.0	0.0	0.0
CBJ	21	4/6/2016	AAE35-2AB	61.7	19	20	26.3	17.0	13.4	2.39	0.7	1.3	0.1	0.1	0.1	0.1	0.1	0.1	0.0	0.0	0.0	0.0
CBJ	22	4/6/2016	AAE35-2BD	59.2	18	19	27.4	17.9	10.0	1.74	0.6	1.2	0.0	0.0	0.0	0.1	0.1	0.1	0.0	0.0	0.0	0.0
CBJ	23	4/6/2016	AAE35-2CB	55.9	18	19	29.9	20.6	3.4	0.60	0.2	0.8	0.0	0.0	0.1	0.1	0.0	0.1	0.0	0.0	0.0	0.0

	Seq.	Meas. date/time	Sample ID	Sum of conc (%)	Proportion (%)	Porpor-tion 2 (%)	CaO	MgO	SiO <sub>2</sub>	Al <sub>2</sub> O <sub>3</sub>	K <sub>2</sub> O	Fe <sub>2</sub> O <sub>3</sub>	TiO <sub>2</sub>	Cl	S	Na <sub>2</sub> O	P <sub>2</sub> O <sub>5</sub>	MnO	SrO	Zn	Cr	Ba	
							Ca	Mg	Si	Al	K	Fe	Ti	Cl	S	Na	P	Mn	Sr	Zn	Cr	Ba	
							(%)	(%)	(%)	(%)	(%)	(%)	(%)	(%)	(%)	(%)	(%)	(%)	(%)	(%)	(%)	(%)	(%)
IGG (dol)	1	8/10/2016 7:41	B36-01B	54.5	41	41	31.9	19.5	2.1	0.43	0.2	0.3	0.0	0.1	0.1	0.0	0.0	0.0	0.0	0.0	0.0	0.0	0.0
IGG (dol)	2	8/10/2016 7:49	B36-02	53.0	28	28	35.0	14.9	2.0	0.40	0.2	0.5	0.0	0.0	0.0	0.0	0.0	0.0	0.0	0.0	0.0	0.0	0.0
IGG (dol)	3	8/10/2016 7:57	B36-03C	57.1	22	22	51.5	0.7	3.0	0.68	0.3	0.7	0.0	0.0	0.1	0.0	0.0	0.0	0.0	0.0	0.0	0.0	0.0
IGG (dol)	4	8/10/2016 8:04	B36-04B	54.8	8	8	39.1	12.6	2.0	0.41	0.2	0.3	0.0	0.0	0.0	0.0	0.0	0.0	0.0	0.0	0.0	0.0	0.0
IBB	33	4/6/2016	AAB27-01	60.5	53	60	40.5	7.5	8.9	1.59	0.8	0.9	0.1	0.0	0.0	0.0	0.1	0.0	0.0	0.0	0.0	0.0	0.0
IBB	34	4/6/2016	AAB27-02	60.1	35	40	31.3	15.7	9.3	1.65	0.8	0.9	0.1	0.0	0.1	0.1	0.1	0.0	0.0	0.0	0.0	0.0	0.0
DGG1	11	4/6/2016	AAE61-01C	52.9	64	66	30.4	21.8	0.3	0.05	0.0	0.2	0.0	0.1	0.0	0.1	0.0	0.0	0.0	0.0	0.0	0.0	0.0
DGG1	12	4/6/2016	AAE61-02	53.5	33	34	30.5	22.0	0.4	0.09	0.0	0.2	0.0	0.1	0.0	0.1	0.0	0.0	0.0	0.0	0.0	0.0	0.0
DBG	13	4/6/2016	AAE42-01C	57.1	41	47	29.6	19.2	6.0	0.95	0.3	0.7	0.0	0.0	0.2	0.0	0.0	0.1	0.0	0.0	0.0	0.0	0.0
DBG	14	4/6/2016	AAE42-02	55.9	29	33	29.7	19.6	4.8	0.63	0.2	0.5	0.0	0.1	0.2	0.1	0.0	0.1	0.0	0.0	0.0	0.0	0.0
DBG	15	4/6/2016	AAE42-03	56.9	18	20	28.6	19.1	7.6	0.64	0.2	0.5	0.0	0.0	0.1	0.0	0.0	0.0	0.0	0.0	0.0	0.0	0.0
DGG2	21	8/10/2016	E58-01B	52.4	45	45	30.1	20.8	1.0	0.17	0.1	0.1	0.0	0.1	0.0	0.0	0.0	0.0	0.0	0.0	0.0	0.0	0.0
DGG2	22	8/10/2016	E58-02B	59.4	33	33	30.8	17.2	8.2	1.39	0.8	0.8	0.1	0.0	0.1	0.0	0.1	0.1	0.0	0.0	0.0	0.0	0.0
DGG2	23	8/10/2016	E58-03	55.7	16	16	30.1	20.6	0.9	0.15	0.1	0.1	0.0	0.1	0.0	0.1	0.0	0.0	0.0	0.0	0.0	0.0	0.0
DGG2	24	8/10/2016	E58-04A	56.8	6	6	30.1	19.9	4.4	1.00	0.7	0.5	0.0	0.0	0.0	0.0	0.0	0.0	0.0	0.0	0.0	0.0	0.0
DBB	1	4/6/2016	AAE52-01D	56.6	33	34	31.9	19.6	3.2	0.71	0.3	0.4	0.0	0.1	0.2	0.1	0.0	0.0	0.0	0.0	0.0	0.0	0.0
DBB	2	4/6/2016	AAE52-02C	56.2	23	24	33.8	18.3	2.6	0.52	0.2	0.4	0.0	0.1	0.1	0.1	0.0	0.0	0.0	0.0	0.0	0.0	0.0
DBB	3	4/6/2016	AAE52-03	58.5	22	23	31.0	18.1	6.5	1.28	0.6	0.7	0.1	0.0	0.1	0.1	0.0	0.0	0.0	0.0	0.0	0.0	0.0
DBB	4	4/6/2016	AAE52-04C	57.3	13	13	31.5	19.4	4.1	0.99	0.4	0.4	0.0	0.1	0.2	0.1	0.0	0.0	0.0	0.0	0.0	0.0	0.0
DBB	5	4/6/2016	AAE52-05B	55.7	6	6	33.9	16.1	3.8	0.87	0.3	0.5	0.0	0.0	0.0	0.0	0.0	0.0	0.0	0.0	0.0	0.0	0.0
						Max	55.3	22.0	40.8	3.07	0.9	1.6	0.1	0.1	0.6	0.5	0.2	0.1	0.1	0.0	0.0	0.0	0.0
						Min	17.3	0.2	0.0	0.01	0.0	0.1	0.0	0.0	0.0	0.0	0.0	0.0	0.0	0.0	0.0	0.0	0.0

Seq.	Meas. date/time	Sample ID	Sum of conc (%)	Proportion (%)	Porpor-tion 2 (%)	CaO	MgO	SiO <sub>2</sub>	Al <sub>2</sub> O <sub>3</sub>	K <sub>2</sub> O	Fe <sub>2</sub> O <sub>3</sub>	TiO <sub>2</sub>	Cl	S	Na <sub>2</sub> O	P <sub>2</sub> O <sub>5</sub>	MnO	SrO	Zn	Cr	Ba	
						Ca	Mg	Si	Al	K	Fe	Ti	Cl	S	Na	P	Mn	Sr	Zn	Cr	Ba	
						(%)	(%)	(%)	(%)	(%)	(%)	(%)	(%)	(%)	(%)	(%)	(%)	(%)	(%)	(%)	(%)	(%)
					Avg	38.9	10.6	5.6	0.72	0.3	0.6	0.0	0.0	0.1	0.1	0.0	0.0	0.0	0.0	0.0	0.0	0.0
					SD	10.8	8.7	7.8	0.68	0.3	0.4	0.0	0.0	0.1	0.1	0.0	0.0	0.0	0.0	0.0	0.0	0.0

Weighted Average																
	CaO	MgO	SiO <sub>2</sub>	Al <sub>2</sub> O <sub>3</sub>	K <sub>2</sub> O	Fe <sub>2</sub> O <sub>3</sub>	TiO <sub>2</sub>	Cl	S	Na <sub>2</sub> O	P <sub>2</sub> O <sub>5</sub>	MnO	SrO	Zn	Cr	Ba
	Ca	Mg	Si	Al	K	Fe	Ti	Cl	S	Na	P	Mn	Sr	Zn	Cr	Ba
	(%)	(%)	(%)	(%)	(%)	(%)	(%)	(%)	(%)	(%)	(%)	(%)	(%)	(%)	(%)	(%)
LGG1	54.6	0.3	0.2	0.06	0.0	0.3	0.0	0.0	0.1	0.1	0.0	0.0	0.0	0.0	0.0	0.0
LGG2	54.7	0.3	0.1	0.03	0.0	0.3	0.0	0.0	0.1	0.0	0.0	0.0	0.0	0.0	0.0	0.0
LMB	49.9	0.5	6.3	1.01	0.3	0.5	0.1	0.0	0.1	0.0	0.0	0.1	0.0	0.0	0.0	0.0
LBG	52.9	0.5	2.3	0.24	0.1	0.3	0.0	0.0	0.1	0.0	0.0	0.0	0.1	0.0	0.0	0.0
LBB1	31.8	3.8	24.1	1.58	0.4	1.0	0.1	0.0	0.2	0.1	0.1	0.1	0.1	0.0	0.0	0.0
LBB2	44.5	1.0	12.6	1.26	0.3	0.6	0.1	0.0	0.1	0.1	0.0	0.0	0.1	0.0	0.0	0.0
IGG	35.1	16.2	2.1	0.39	0.2	0.5	0.0	0.0	0.0	0.0	0.0	0.0	0.0	0.0	0.0	0.0
IGB1	34.4	14.7	6.4	1.1	0.6	0.8	0.0	0.0	0.1	0.1	0.0	0.0	0.0	0.0	0.0	0.0
CBJ	29.4	18.5	6.3	1.14	0.4	1.0	0.0	0.0	0.1	0.1	0.1	0.1	0.0	0.0	0.0	0.0
IGG (dol)	37.7	13.4	2.3	0.5	0.2	0.4	0.0	0.0	0.0	0.0	0.0	0.0	0.0	0.0	0.0	0.0
IBB	36.9	10.8	9.0	1.61	0.8	0.9	0.1	0.0	0.1	0.0	0.1	0.0	0.0	0.0	0.0	0.0
DGG1	30.4	21.8	0.3	0.06	0.0	0.2	0.0	0.1	0.0	0.1	0.0	0.0	0.0	0.0	0.0	0.0
DBG	29.4	19.3	5.9	0.78	0.2	0.6	0.0	0.0	0.2	0.0	0.0	0.0	0.0	0.0	0.0	0.0
DGG2	30.3	19.5	3.6	0.6	0.3	0.4	0.0	0.1	0.0	0.0	0.0	0.0	0.0	0.0	0.0	0.0
DBB	32.2	18.7	4.0	0.84	0.3	0.5	0.0	0.1	0.2	0.1	0.0	0.0	0.0	0.0	0.0	0.0